

Polyphase ductile/brittle deformation along a major tectonic boundary in an ophiolitic nappe, Alpine Corsica: Insights on subduction zone intermediate-depth asperities



Rémi Magott ^{a,*}, Olivier Fabbri ^a, Marc Fournier ^b

^a Laboratoire Chrono-environnement UMR CNRS 6249, Université Bourgogne Franche-Comté, F-25000 Besançon, France

^b Sorbonne Universités, UMR 7193, UPMC Univ. Paris VI, ISTEP, F-75005 Paris, France

ARTICLE INFO

Article history:

Received 20 August 2016

Received in revised form

2 December 2016

Accepted 6 December 2016

Available online 9 December 2016

Keywords:

Alpine Corsica

Pseudotachylyte

Mylonite

Metagabbro

Peridotite

Serpentinite

Asperity

ABSTRACT

In an ophiolitic nappe of Alpine Corsica, a major fault zone superimposes metagabbro over serpentinite and peridotite. Ductile and brittle deformation structures are observed in the fault damage zones. In the metagabbro damage zone, early deformation culminates in blueschist or eclogite facies conditions and consists of west-verging mylonitization alternating with pseudotachylyte-forming faulting with undetermined vergence. This early deformation is likely coeval with west-verging seismic (pseudotachylyte-forming) reverse faulting in the footwall peridotite or with aseismic distributed cataclastic deformation of footwall serpentinite. These early events (aseismic mylonitization or distributed cataclasis and seismic faulting) are interpreted as reverse faulting/shear in an east-dipping subducting oceanic lithosphere in Cretaceous to Eocene times. Late deformation events consist of ductile shear and seismic faulting having occurred under retrograde greenschist conditions. Kinematics of the ductile shear is top-to-the-east. These events are interpreted as the result of syn-to post-collision extension of Alpine Corsica in Eocene to Miocene times. The heterogeneous distribution of pseudotachylyte veins along the fault zone (abundant at peridotite–metagabbro interfaces, rare or absent at serpentinite–metagabbro interfaces) is interpreted as the consequence of contrasted frictional properties of the rocks in contact. High-friction peridotite–metagabbro contacts could correspond to asperities whereas low-friction serpentinite–metagabbro contacts could correspond to creeping zones.

© 2016 Elsevier Ltd. All rights reserved.

1. Introduction

Subduction zone seismicity is a major concern in terms of seismic hazard assessment and mitigation. Indeed, on average, it accounts for more than 85% of the seismic energy released in the world (Scholz, 2002). Particularly worrisome are seismic ruptures at the plate interface, at depths shallower than 60 km (so-called shallow depth seismicity, Frohlich, 2006). Such ruptures are able to trigger giant tsunamis that can add to devastation resulting from ground shaking (Satake and Tanioka, 1999). Though less concerning than the shallow one, intermediate-depth seismicity, with hypocenters between 60 and 300 km, still constitutes a major threat in coastal areas, either through direct shaking (Frohlich, 2006) or through indirect loading of shallower close-to-failure faults (e.g.,

Astiz et al., 1988).

Earthquake studies indicate that seismic rupture surfaces are not homogeneous but are constituted of patches or domains with contrasted physical characteristics. Such heterogeneities, basically taken into account in the concepts of asperities or barriers, are observed in intra-plate as well as in inter-plate seismic fault surfaces (Das and Aki, 1977; Kanamori and Stewart, 1978; Aki, 1979; Lay and Kanamori, 1981; Lay et al., 1982; Bakun and McEvelly, 1984; Nadeau et al., 1995; Igarashi et al., 2003; Seno, 2003; Yamanaka and Kikuchi, 2004; Bürgmann et al., 2005; Semmane et al., 2005). Heterogeneities are tentatively characterized by differences in earthquake physical parameters such as coseismic slip, seismic moment release, stress drop, seismic coupling ratio, frictional properties (friction coefficient or rate-and-state dependent friction law $a - b$ parameter, Gutenberg-Richter law b parameter) or pore pressure. Some asperities seem to be spatially persistent, at least at the scale of several years or several tens of years (Bakun and McEvelly, 1984; Nadeau et al., 1995; Igarashi et al., 2003; Okada

* Corresponding author.

E-mail address: remi.magott@univ-fcomte.fr (R. Magott).

et al., 2003; Hasegawa et al., 2007). Such a spatial persistency suggests that the location of asperities is, at least partly, controlled by specific rocks that in turn likely influence the values of the above-mentioned physical parameters. In subduction zones, asperities are mostly described along the plate interface seismogenic zone (megathrust) of the upper 50–60 km. At depths larger than 60 km, asperities are less commonly reported and are poorly localized (Igarashi et al., 2003; Hasegawa et al., 2007; Legrand et al., 2012).

Pseudotachylytes containing blueschist to eclogite facies mineral assemblages are considered to result from earthquake faulting at intermediate to large depths in subduction zones (Austrheim and Boundy, 1994; Lund and Austrheim, 2003). Their study can thus provide insights on the physical or chemical processes that trigger, accompany or follow intermediate-depth seismic ruptures (John and Schenk, 2006; Andersen et al., 2008, 2014; John et al., 2009). An example of such blueschist to eclogite facies pseudotachylytes likely formed in a subduction zone framework is provided by the Corsican occurrences initially reported by Austrheim and Andersen (2004) and subsequently analyzed from the petrographic, mineralogical or structural points of view by Andersen and Austrheim (2006), Andersen et al. (2008, 2014), Deseta et al. (2014a and b), Magott et al. (2016) and Ferré et al. (2016). The paleo-seismic veins are distributed in the vicinity of a major fault surface separating oceanic crust rocks from oceanic mantle rocks.

The aim of this paper is two-fold. First, the relative chronology and the kinematics of the deformation episodes recorded in oceanic crust rocks are analyzed and then compared with the results of Magott et al. (2016) obtained in the mantle rocks. These investigations allow to distinguish aseismic ductile shear events and seismic faulting events which, for the earliest of them, took place in a subducting slab at depths around 60 km. Second, the presence or absence of seismic slip evidence is tentatively related to contrasts in friction of rocks that are in contact along faults. This tentative correlation provides information about the lithological nature of areas with strong coupling (asperities) vs. areas with weak coupling, thus suggesting a possible geological explanation for fault surface heterogeneities detected by seismological observations.

2. Geological setting

2.1. Geological setting of Alpine Corsica

Three main types of tectonic units are recognized in the Corsican segment of the Alpine-Apennine orogenic system (Mattauer and Proust, 1976; Faure and Malavieille, 1981; Mattauer et al., 1981; Jolivet et al., 1990, 1991; Fournier et al., 1991; Molli and Malavieille, 2011; Vitale-Brovarone et al., 2013, 2014): (i) the *Schistes Lustrés* units (Tethysian ophiolitic rocks and their sedimentary cover), (ii) the Corsica continental margin units (Variscan plutonic and volcanic rocks), and (iii) the *Nappes Superficielles* or Upper Nappes (ophiolitic units and various sedimentary rocks).

The stacking or imbrication of ophiolites and continental margin-derived units is classically interpreted as the result of an Eocene collision between the Apulian and European continental blocks following an east-dipping subduction of the Piemonte-Liguria Ocean and its ocean-continent transition zone in Cretaceous to Early Tertiary times (Mattauer and Proust, 1976; Mattauer et al., 1977, 1981; Fournier et al., 1991; Jolivet et al., 1991; Meresse et al., 2012; Vitale-Brovarone et al., 2013; Lagabrielle et al., 2015). More complex models call for a shift from the east-dipping 'Alpine' subduction of the Piemonte-Liguria Ocean to a west-dipping subduction, either intra-oceanic or beneath a continental or island-arc microblock (Guerrera et al., 1993; Malavieille et al., 1998; Durand-

Delga and Rossi, 2002; Molli and Malavieille, 2011; Turco et al., 2012).

Most of the Corsica Alpine units underwent a HP/LT (blueschist to lawsonite-eclogite facies) metamorphism, associated to a top-to-the-west kinematics (Lahondère, 1996; Vitale-Brovarone et al., 2013). This HP/LT metamorphism is considered to result from the Alpine subduction during Eocene (55–34 Ma, Brunet et al., 2000; Martin et al., 2011; Maggi et al., 2012). Vitale-Brovarone and Herwartz (2013) suggested that the metamorphic peak could be between 34 and 37 Ma. A late retrograde greenschist facies metamorphic event occurred during the exhumation of Alpine Corsica in the Oligocene-Miocene. This event is associated with non-coaxial top-to-the-east ductile shear (Jolivet et al., 1990, 1991; Fournier et al., 1991; Brunet et al., 2000; Rossetti et al., 2015).

2.2. Study area

The study area is located around the Cima di Gratera peak and consists of an ophiolitic nappe thrust over continental units (so-called Mordeda-Farinole and Pigno-Olivaccio units, Lahondère, 1996; Meresse et al., 2012) through a fault zone labelled φ_1 (Fig. 1). The nappe, referred to as the Cima di Gratera nappe, is a part of the *Schistes Lustrés* complex and is composed of two units: a lower ultramafic unit consisting of serpentinite including decameter to hectometer-scale elliptical masses of variably serpentinitized peridotite, and an upper mafic unit composed of metagabbro. The contact between the two units is a fault surface referred to as φ_2 .

2.3. The ultramafic unit

The ultramafic unit consists predominantly of massive serpentinite (former peridotite with a volume proportion of serpentinitization > 80%). However, decameter to hectometer-scale masses of fresh to moderately serpentinitized peridotite are locally preserved in the serpentinite. The fresh peridotite is composed of olivine (Fo₈₄), clinopyroxene, enstatite and minor plagioclase, Cr-spinel and magnetite, with the modal proportions of a plagioclase Iherzolite (Deseta et al., 2014a). In moderately serpentinitized peridotite, olivine is replaced by serpentine, talc and magnetite. Serpentinite is composed of serpentine, talc, magnetite and pyroxene, the latter being almost entirely recrystallized into bastite. Raman spectroscopy indicates that serpentine mostly consists of antigorite (Magott, 2016).

Most peridotite masses are located in the center or to the west of the study area and immediately beneath φ_2 (Fig. 1). Rare pyroxenite and gabbro dykes were observed in the peridotite near φ_2 . Foliated serpentinite is found locally at the top of the unit, immediately beneath φ_2 (see below, C type deformation zone) or scattered within the median part of the unit, away from φ_2 .

According to Deseta et al. (2014a), the peridotite underwent two greenschist facies metamorphic events leading to partial recrystallization of diopside and enstatite to tremolite and actinolite, and of olivine to talc and serpentine. The first metamorphic event is related to the hydrothermal alteration associated with the ocean-continent-transition extension. The second metamorphic event is interpreted as retrograde metamorphism during syn- to post-collision extension (Deseta et al., 2014a). Because the peridotite composition does not allow the formation of medium- to high-pressure diagnostic mineral assemblages, it is impossible to ascertain whether the ultramafic unit underwent a HP/LT metamorphism or not.

Peridotite is crossed by numerous pseudotachylyte fault veins (Andersen and Austrheim, 2006; Andersen et al., 2008, 2014; Deseta et al., 2014a; Magott et al., 2016). Most of them are flat-lying and are

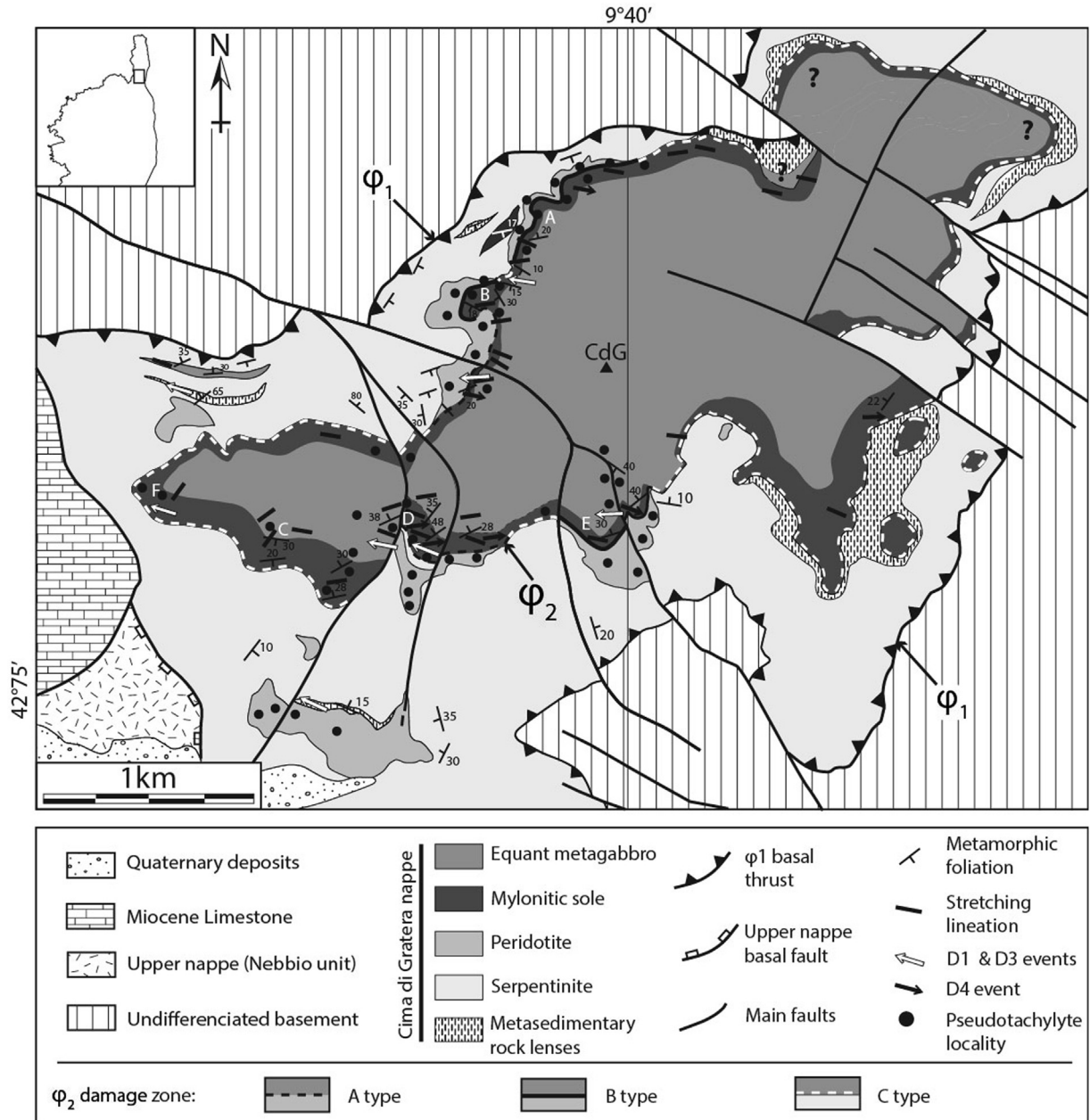


Fig. 1. Structural map of the Cima di Gratera nappe (after Faure and Malavieille, 1981; Lahondère, 1996; Meresse et al., 2012 and our observations). CdG is for Cima di Gratera summit. Localities A to F refer to measurement sites of Fig. 7.

parallel to ϕ_2 . The volume of pseudotachylyte veins increases toward the contact. Immediately below ϕ_2 , the proportion of melted rock can reach about 75% in volume. As depicted in Andersen and Austreim (2006), Andersen et al. (2014) and Magott et al. (2016), such zones, up to 150 m thick, show complex and anastomosed networks of fault veins. The length of the fault veins is between 1 and 10 m and their thickness generally does not exceed 1.5 cm (although up to 10 cm thick veins are locally observed).

Steeply-dipping (ca. 55°E) N20 to N40°E pseudotachylyte-bearing fault zones are developed at distance from ϕ_2 . Close to ϕ_2 , the steeply dipping veins tend to be obliterated by the flat lying ones. Peridotite hosting pseudotachylyte veins is cataclastic (Magott et al., 2016). Cataclasis predates frictional melting.

No pseudotachylyte vein could be found in the foliated serpentinite, whatever the latter is located in the middle part of the

ultramafic unit or immediately below ϕ_2 . Besides, where the serpentinite is not foliated, pseudotachylyte veins are present, although serpentinitized to various degrees. In these occurrences, serpentinitization post-dates pseudotachylyte formation. At the microscopic scale, this relative chronology is confirmed by widespread partly or entirely serpentinitized olivine or pyroxene microclasts or survivor clasts (Fig. 2).

2.4. The mafic unit

Most of the mafic unit corresponds to a massive or locally layered equant metagabbro which can be coarse-grained (crystal lengths up to 15 mm) or fine-grained (crystal lengths less than 2 mm). The primary (magmatic) mineralogical composition of the metagabbro consists of commonly sericitized plagioclase (An_{92}),

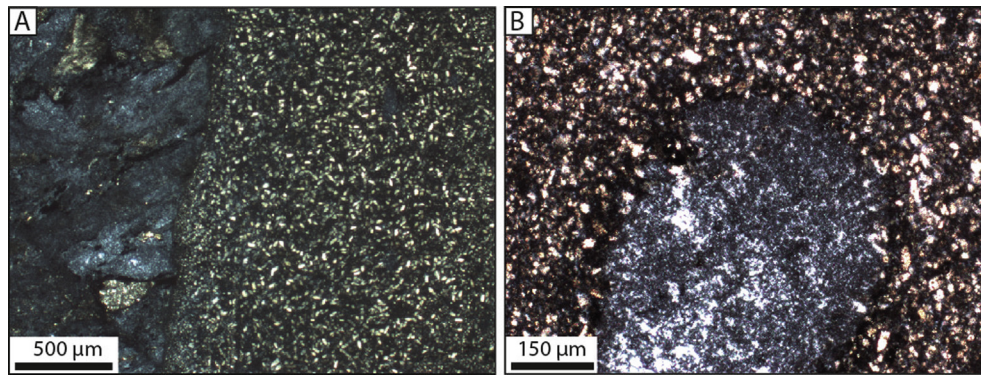


Fig. 2. Photomicrographs showing that serpentinization post-dates pseudotachylyte formation in the Cima di Gratera ultramafic unit (locality D). A: serpentinized host peridotite (left) crossed by a pseudotachylyte vein (center and right). The vein contains numerous white, lath-shaped microlites which consist of antigorite and which result from serpentinization of olivine or pyroxene. The chilled margin in the central part of the photograph is characterized by smaller microlites than in the rest of the vein. B: serpentinized olivine or pyroxene survivor clast embedded in an antigorite microlite-laden pseudotachylyte (same vein as A). Note the roundness of the clast and the embayment at the upper left side of it.

clinopyroxene (diopside and augite), minor olivine (F₉₀) and ilmenite. According to Deseta et al. (2014a), the mafic unit suffered from three metamorphic events which are: (1) an early greenschist facies event associated with the partial replacement of pyroxene by actinolite, tremolite, Mg-hornblende and clinocllore, and with partial or total replacement of olivine by serpentine, magnetite and iddingsite. (2) A HP/LT metamorphic event characterized by the substitution of pyroxene, tremolite, actinolite and Mg-hornblende by glaucophane, omphacite, barroisite and clinozoisite, and the substitution of plagioclase by albite. (3) A late greenschist facies metamorphic event corresponding to crystallization of tremolite, clinocllore, epidote, pumpellyite and albite on all pre-existing minerals, including those formed during the two above-mentioned events. The highest pressure/temperature metamorphic conditions recorded in the Cima di Gratera nappe correspond to blueschist to low-grade eclogite facies of the second metamorphic event, as attested by the presence of glaucophane and omphacite in the mafic unit (Deseta et al., 2014a). According to these authors, the peak temperature conditions range from 430 to 550 °C and the peak pressure conditions range from 1.8 GPa to 2.6 GPa. These ranges are similar to those obtained by Vitale-Brovarone et al. (2013) in nearby units, namely 414–471 °C and 1.9–2.6 GPa.

The basal part of the mafic unit, which will be referred to as the mylonitic sole, consists of a mylonitic metagabbro (Fig. 1) whose thickness varies from a few centimeters to about 30 m. The transition between the equant metagabbro and the mylonitic metagabbro is progressive and takes place over a few meters. Above the mylonitic sole, the equant metagabbro is crossed by flat-lying to gently dipping mylonitic shear zones which can followed laterally over several tens of meters. Their thickness generally does not exceed 50 cm. In the localities where the junction is exposed, the secondary shear zones merge with the mylonitic sole.

2.5. The φ_2 contact and the different damage zone types

The φ_2 contact consists of a sharp planar or gently undulating striated surface. On either side of this surface, the rock is brecciated over a few millimeters. Striations borne by this surface trend around N120°E. Sense of slip is undetermined. Differences between rock types of the hanging-wall and footwall of the φ_2 fault surface allow to map three different types of damage zones (DZs) labelled A, B and C (Figs. 1 and 3).

2.5.1. A type DZ

A type DZ (Figs. 3A and 4) superimposes mylonitic metagabbro over pseudotachylyte-rich peridotite. The mylonitic metagabbro also includes pseudotachylyte veins, but much less than in the footwall. These pseudotachylyte veins will be described below (Section 3.2). The A type DZ is characterized by a 0.5–1.5 m thick pseudotachylyte layer intercalated between the mylonitic gabbro and the pseudotachylyte-rich peridotite (Figs. 3A and 4) and consisting of an imbrication of a large number of centimeter- or millimeter-thick fault veins and injection veins. This characteristic layer, referred to as *intermediate pseudotachylyte*, was already reported by Andersen et al. (2014; see Fig. 3 therein). The φ_2 surface is located between this intermediate pseudotachylyte and the overlying metagabbro (Fig. 4A). The contact between the intermediate pseudotachylyte and the lower peridotite is not faulted. It is a classical pseudotachylyte-host rock intrusive contact.

At the outcrop scale, the intermediate pseudotachylyte is characterized by the presence of numerous rounded mylonitic metagabbro clasts whose dimensions are between 1 and 10 cm (Fig. 4C). Some clasts contain pre-brecciation pseudotachylyte veins abutting against the clast-matrix contact. The clasts are embedded in a dark green to dark blue pseudotachylyte matrix (Fig. 4D). At the microscopic scale, the pseudotachylyte matrix consists of a series of intermingled fault or injection veins, some of them being partly cataclastic, some others cutting the veins having suffered from cataclasis. In some instances, up to 4 stages of vein formation (that is, frictional melting) can be counted, alternating or not with cataclastic events. This estimate is conservative and the actual number of frictional melting events is probably larger. Due to cataclasis and subsequent alteration or weathering, it is uneasy to identify all the pseudotachylyte veins. However, the following observations can be ascertained.

- (1) Some veins consist almost only of serpentine occurring as needles or as polygonal crystals. Minor greenschist-facies amphibole (possibly tremolite) is also observed. Survivor clasts are rounded and thoroughly serpentinized. Despite the lack of glass (possibly devitrified) or microlites (possibly serpentinized), these veins are interpreted as pseudotachylyte veins. They likely result from frictional melting of the peridotite, before subsequent pervasive serpentinization, the latter being favored by late fluid flow.
- (2) Some veins include omphacite microlites and are interpreted as resulting from frictional melting of the metagabbro under

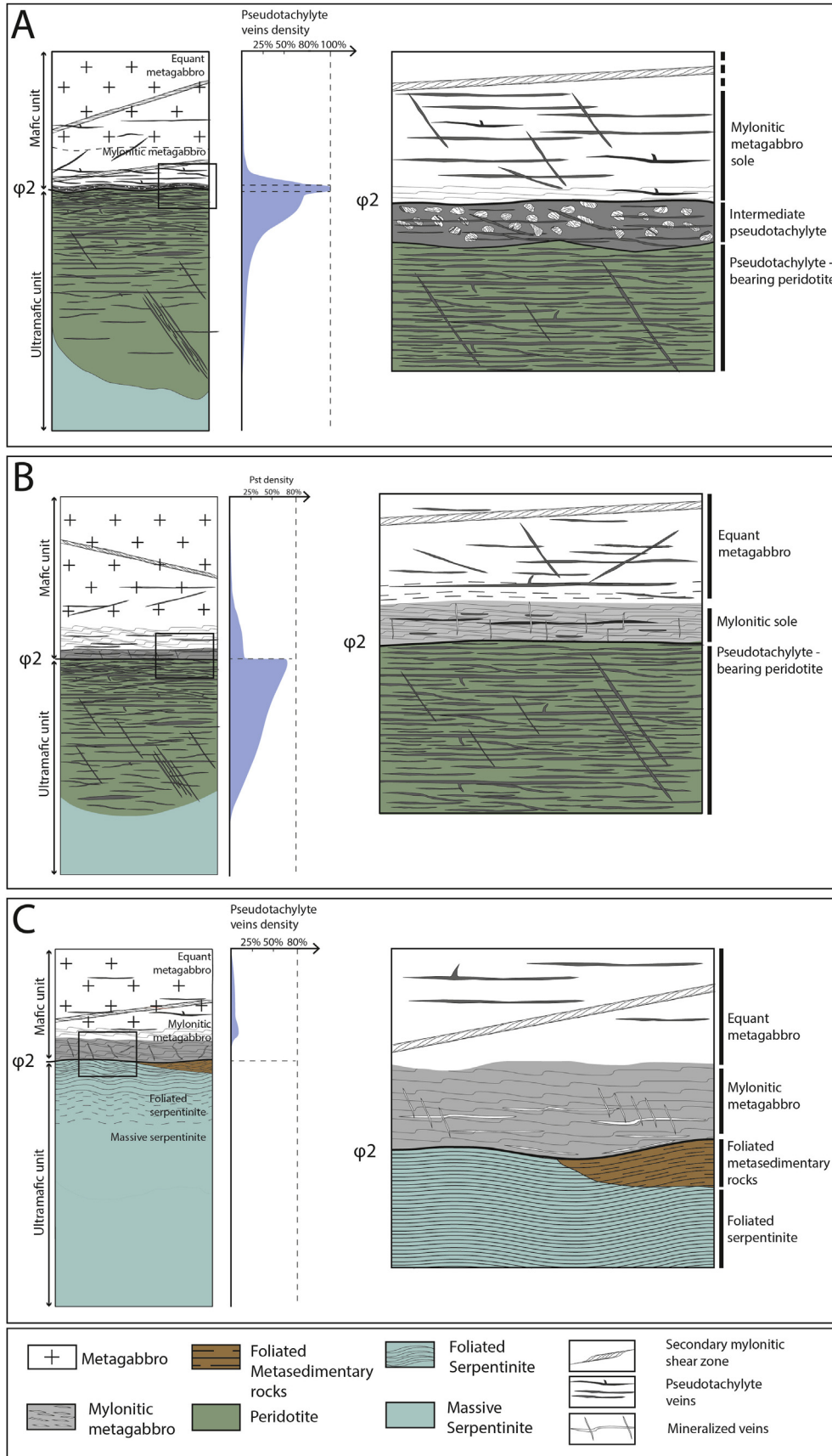


Fig. 3. Schematic sections across the three types of DZs around ϕ_2 along with estimated pseudotachylyte vein density. A: A type DZ between mylonitic metagabbro and pseudotachylyte-rich peridotite, with intermediate pseudotachylyte between. The density of the peridotite-hosted pseudotachylyte fault veins increases toward the contact. B: B type DZ between mylonitic metagabbro and pseudotachylyte-rich peridotite. C: C type DZ between mylonitic metagabbro and either foliated serpentinite or metasedimentary rock. In C type DZ, pseudotachylyte veins are observed neither in the hanging-wall nor in the footwall of ϕ_2 .

eclogite facies conditions. These veins include survivor clasts of clinopyroxene and plagioclase, and also of pseudotachylyte (Fig. 5). They can be reworked together with their host metagabbro clasts, or can be secant to the clasts and to older veins.

- (3) Lastly, some veins contain tremolite + Mg-hornblende microlites and clinopyroxene survivor clasts, and therefore result from frictional melting of the metagabbro, but under greenschist facies conditions. These veins crosscut all other veins, especially the omphacite-bearing ones. They are among the latest formed.

In summary, the intermediate pseudotachylyte is the final result of a number of brittle deformation events mixing frictional melting events and cataclastic events. The veins containing omphacite microlites, which are among the oldest, were formed under eclogite facies conditions while the youngest frictional events occurred under greenschist facies conditions. Both the above-lying metagabbro and the underlying peridotite supplied melt to the intermediate pseudotachylyte.

2.5.2. B type DZ

Like the A type DZ, the B type DZ superimposes mylonitic metagabbro over pseudotachylyte-rich peridotite. However, it lacks the intermediate pseudotachylyte (Figs. 3B and 4). Moreover, the metagabbro contains thin (thickness < 1 mm) albite veins parallel or oblique to the foliation. The veins postdate both the foliation and the pseudotachylyte veins. Their filling consists exclusively of granular albite.

2.5.3. C type DZ

The C type DZ consists of a direct superimposition of mylonitic metagabbro over foliated serpentinite or, less commonly, over metasedimentary rocks (Figs. 3C and 4). Another conspicuous difference with the two other DZ types (especially with the A type one) is the presence of abundant mineralized veins in the mylonitic metagabbro. The foliation in the serpentinite below ϕ_2 is regular, finely spaced and parallel to ϕ_2 . Optical microscope observation suggests that the serpentinite foliation results from distributed cataclastic flow, without clear crystal plastic deformation, similarly to the observations made on experimentally deformed serpentine samples at pressures up to 1000 MPa and room temperature (Escartin et al., 1997). With increasing distance from ϕ_2 , the foliation tends to be less regular and more loosely spaced, before disappearing. At distances of about 20–30 m, the serpentinite is massive. In the localities where the footwall consists of metasedimentary rocks (marbles, meta-radiolarites, pelitic schists, basic schists), the foliation is parallel to that of the metagabbro. Near ϕ_2 , pseudotachylyte veins could be found neither in the serpentinite, whatever foliated or massive, nor in the metasedimentary rocks. The foliation of the mylonitic metagabbro is parallel or slightly oblique (<5°) to ϕ_2 . No pseudotachylyte vein could be found in the mylonitic metagabbro. Conversely, the hanging-wall of C type DZ shows abundant mineralized veins, either coeval with the ductile deformation or post-dating it. The oldest veins consist of glaucophane + plagioclase (mostly albite) assemblages. These veins are deflected, folded or stretched, showing that they suffered from ductile deformation. The most widespread veins, which crosscut the previous ones, are filled with epidote + clinocllore + actinolite + tremolite. These veins are locally folded, but folding intensity is weaker than for the glaucophane/plagioclase veins. The youngest veins consist of albite + epidote assemblages. They are parallel or slightly oblique to the foliation. They are never folded nor deflected, and are secant on all above-mentioned veins. Their thickness can reach 2 mm,

whereas that of the other types does not exceed 1 mm.

3. Deformation structures in the mafic unit deformation zone

3.1. Ductile deformation structures

The foliation of the mylonitic metagabbro (sole and secondary mylonitic shear zones) is most frequently parallel to ϕ_2 , though oblique relationships are also observed. At the microscopic scale, the foliation is defined by ductilely flattened plagioclase or by a preferred orientation of pyroxene. Plagioclase porphyroclasts are flanked by hornblende and glaucophane overgrowths themselves partially overprinted by tremolite + clinocllore + epidote assemblages. Clinopyroxene porphyroclasts are flanked by overgrowths of tremolite, clinocllore and minor omphacite.

The foliation of the mylonitic metagabbro bears a mineral and stretching lineation whose trend is predominantly between N80 and N140°E and whose plunge is between 10 and 40° eastward (Fig. 6). More precisely, two lineation clusters can be distinguished, one with trends around N80°E and another one with trends around N120°E. As will be detailed in Section 5, the kinematic analysis allows to distinguish between two sets of lineation corresponding to the two directional clusters, namely the N80°E set and the N120°E set. Indeed, at the microscopic scale, thin sections parallel to N80°E indicate predominantly top-to-the-east shear senses whereas thin sections parallel to N120°E indicate predominantly top-to-the-west shear senses. In the field, it is not possible to differentiate the two sets of lineation on the basis of mineralogical criteria because both are outlined by elongated plagioclase porphyroclasts and by hornblende crystals aligned following their longest dimension.

3.2. Pseudotachylyte veins

3.2.1. Veins in mylonitic metagabbro (sole and secondary mylonitic shear zones)

Two sets of pseudotachylyte fault veins are preserved in the mylonitic metagabbro. The first set was formed before mylonitization. Fault veins of this set are boudinaged and never exceed 1.5 cm in length and 0.5 cm in thickness. At the microscopic scale, the survivor clasts are flattened and flanked by overgrowths of fibrous omphacite. The matrix is foliated and microlites are not recognizable. The second set of fault veins is not ductilely deformed and therefore post-dates mylonitization. Veins of this set are between 1 and 10 mm thick (see Fig. 12B in Magott et al., 2016). Fig. 7 shows the attitudes of post-mylonitization fault veins in the mylonitic sole. Most veins dip gently to moderately, but the dipping directions are scattered. At the microscopic scale, plagioclase and pyroxene survivor clasts are embedded in a microlitic matrix. Microlites consist of acicular Mg-hornblende, tremolite and actinolite (Fig. 8).

3.2.2. Veins in equant metagabbro

In the equant metagabbro, pseudotachylyte fault veins are abundant, but their density decreases upwards with increasing distance to the contact. Fig. 7 shows that fault veins are either flat-lying to gently dipping or moderately to steeply dipping. Such a geometry is reminiscent of what is observed in the ultramafic unit where flat-lying veins coexist with steeply-dipping veins (Andersen and Austrheim, 2006; Magott et al., 2016).

Based on microscopic observations and on microprobe analyses (Table 1), two types of pseudotachylyte veins can be distinguished in the equant metagabbro: omphacite-bearing veins are characterized by microlites of Al-rich omphacite and anorthite (as already described by Austrheim and Andersen, 2004; Deseta et al., 2014a

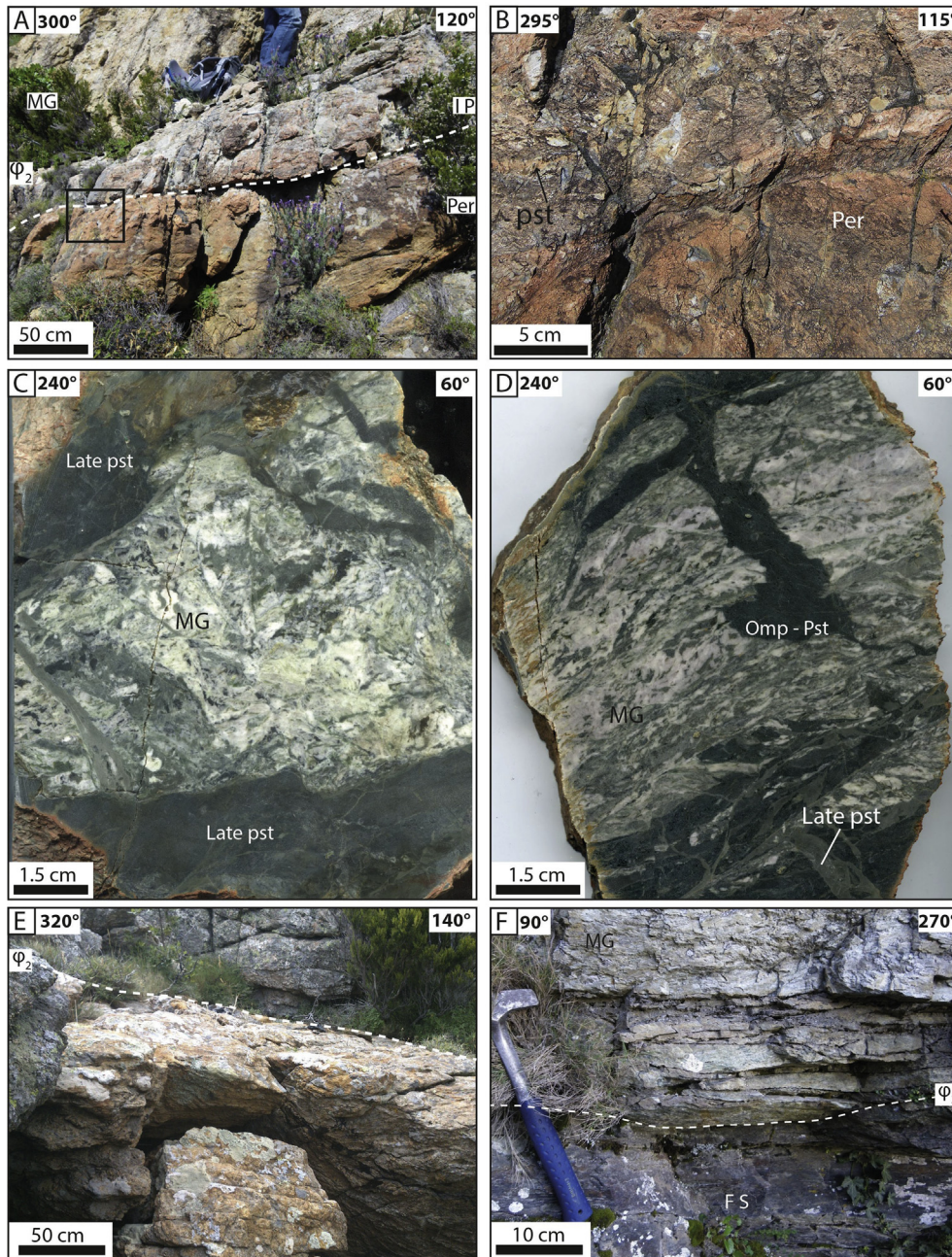


Fig. 4. Field and hand sample aspect of the relationships between ϕ_2 hanging-wall and footwall DZs. A: A type DZ across ϕ_2 showing, from top to bottom, the mylonitic metagabbro (MG) of the mafic unit, the intermediate pseudotachylyte (IP), and the pseudotachylyte-rich peridotite (Per). B: closer view (rectangle in A) showing the clast-laden intermediate pseudotachylyte (IP) and the underlying peridotite (Per). C: hand sample section showing a metagabbro clast (MG) embedded in a pseudotachylyte matrix (pst). The clast itself is crossed by older omphacite-bearing pseudotachylyte veins. D: hand sample section showing a metagabbro clast (MG) crossed by omphacite-bearing pseudotachylyte veins (Omp-pst) injected from the surrounding 'matrix'. E: B type DZ showing foliated metagabbro overlying pseudotachylyte-rich peridotite. F: C type DZ showing foliated metagabbro (MG) overlying foliated serpentinite (FS). Note the lack of pseudotachylyte veins on either side of ϕ_2 .

and b), and amphibole-bearing veins characterized by microlites of acicular to skeletal Mg-hornblende, tremolite and actinolite. Amphibole-bearing veins unambiguously crosscut omphacite-bearing veins (Fig. 8C) and are therefore younger.

4. Metamorphic conditions in the mafic unit deformation zone

4.1. Mylonitic metagabbro

At the thin section scale, the succession of three episodes of

metamorphism (greenschist facies \rightarrow blueschist to eclogite facies \rightarrow greenschist facies) reported by Deseta et al. (2014a) is recognized in the mylonitic metagabbro. Some asymmetric pressure shadows are made of fibrous assemblages of tremolite and clinoclone while others consist of glaucophane, plagioclase and omphacite. Mg-hornblende resulting from the greenschist facies metamorphism of pyroxene can be flanked by asymmetric recrystallizations of assemblages of glaucophane, plagioclase and omphacite, indicating that the greenschist facies metamorphic event was followed by a blueschist to eclogite facies metamorphic event. Conversely, in some instances, blueschist to eclogite facies

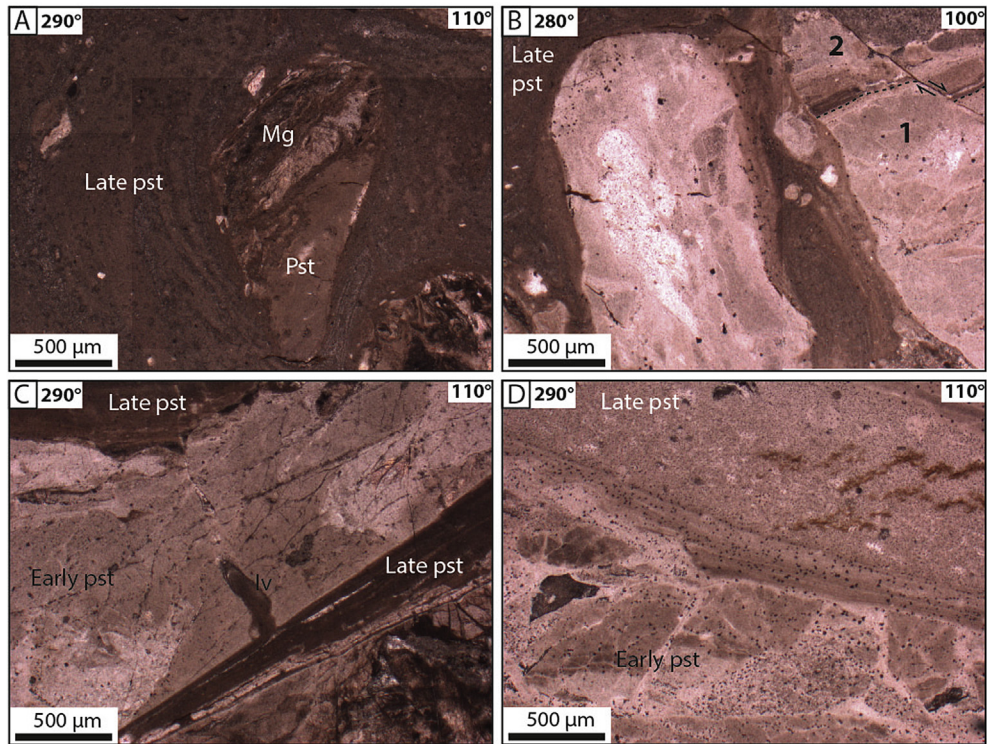


Fig. 5. Photomicrographs showing typical features of the intermediate pseudotachylyte of A type DZ. A: pseudotachylyte reworking a survivor clast composed of metagabbro (Mg) and pseudotachylyte (Pst). B: clasts of pseudotachylyte embedded in a pseudotachylyte matrix. The clast to the right is itself composed of a young vein (2) crossing an older vein (1). Note the chilled margin of vein 2 and the minor fault offsetting it. C: Late pseudotachylyte veins intruded on both sides of an early fault vein. The two generations of veins are supposed to result from gabbro melting. Note the fracture network crossing the early vein. D: Late pseudotachylyte vein intruded through an early fault vein. Note the abundant iron hydroxides (dark dots). The two veins are supposed to result from melting of the metagabbro.

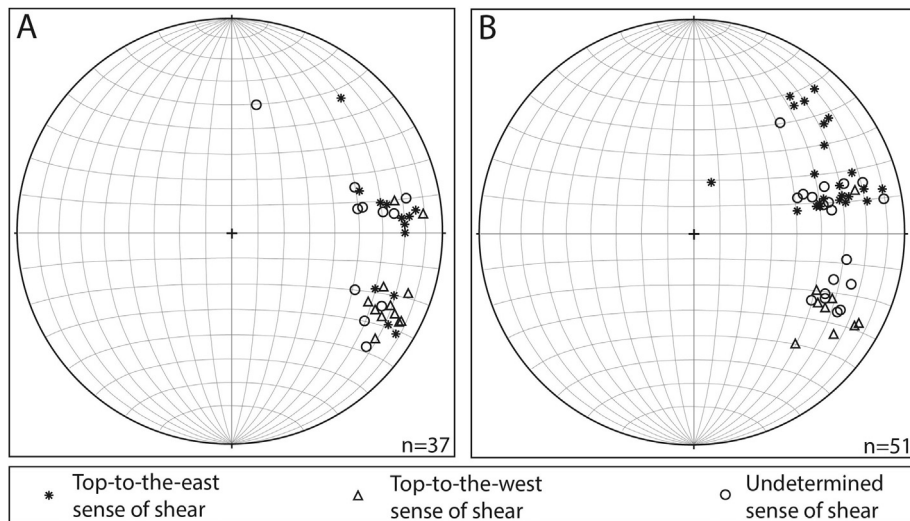


Fig. 6. Lower-hemisphere equal-area projection of the mineral and stretching lineation in the mafic unit and associated senses of shear. A: basal mylonitic sole. B: secondary mylonitic shear zones.

assemblages are overprinted by greenschist facies mineral assemblages consisting of tremolite, clinocllore and clinozoisite.

4.2. Pseudotachylyte veins

Microscopic observations and microprobe analyses indicate that the *pre-mylonitization veins* were *ductilely deformed* under eclogite-facies conditions, as indicated by omphacite overgrowths in

pressure shadows flanking survivor clasts (Fig. 9). At the microscopic scale, the veins of this set show flattened and elongated plagioclase clasts flanked by omphacite overgrowths. *Post-mylonitization veins* were formed in greenschist facies conditions, as attested by Mg-hornblende, tremolite and actinolite microlites (see above).

Since they contain the same microlite assemblages, the pseudotachylyte veins of the second set of both the mylonitic sole and

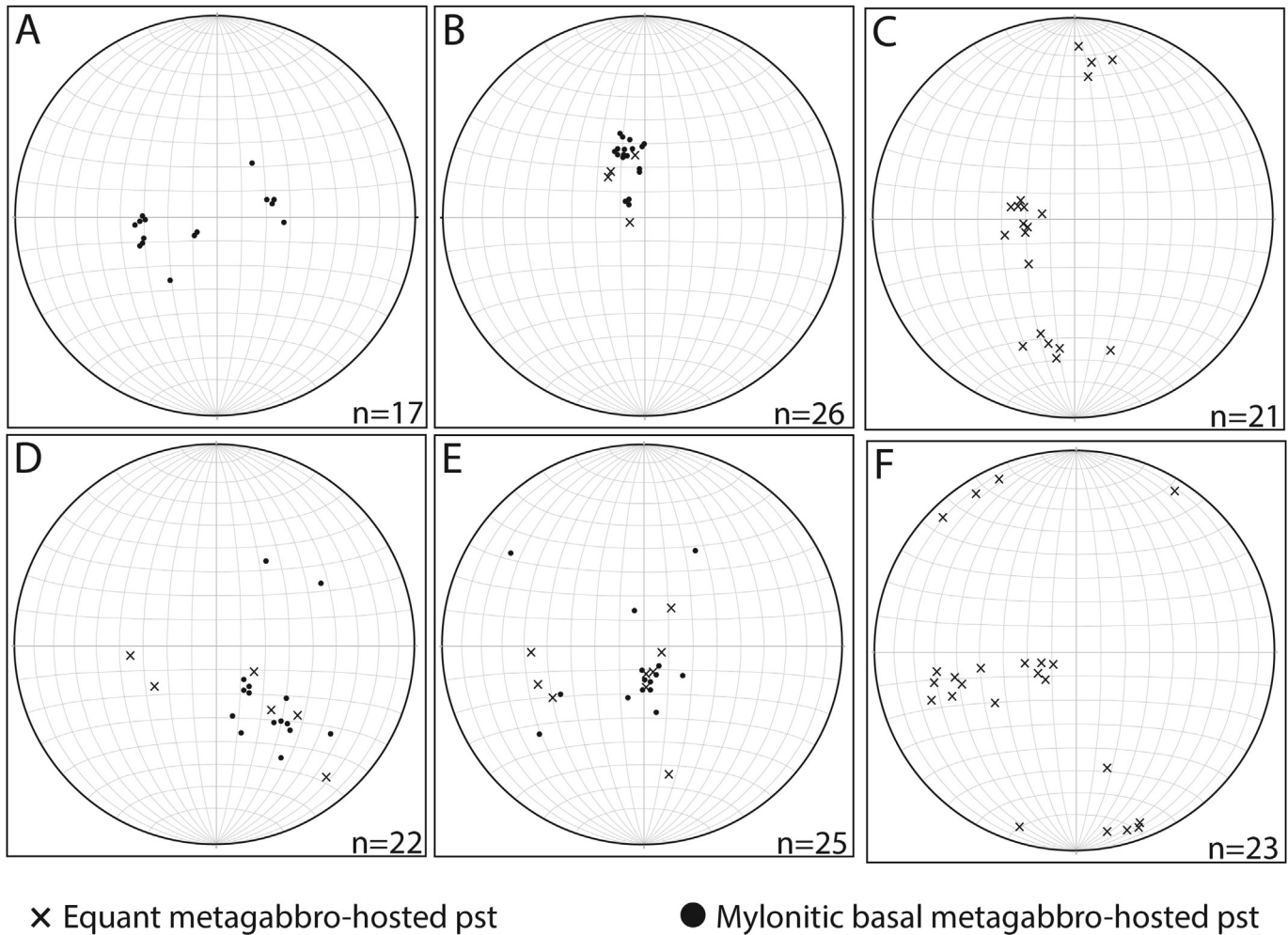


Fig. 7. Poles to pseudotachylyte veins in the equant metagabbro and post-mylonitization pseudotachylyte veins in the mylonitic metagabbro. See Fig. 1 for measurement locations.

the overlying equant metagabbro possibly formed coevally in greenschist facies conditions. Besides, the first (older) set of veins in the equant metagabbro was formed under the same eclogite facies conditions as the ductile deformed veins of the mylonitic sole. Here again, both types of veins could have been formed coevally, but this synchronicity cannot be further ascertained.

5. Kinematics in the mafic unit deformation zone

5.1. Ductile deformation structures

Fig. 6 shows that the mineral and stretching lineation in the mylonitic metagabbro of the sole and the secondary shear zones falls into two clusters, one around N80°E and another one around N120°E. Thin sections parallel to the N120°E lineation show criteria such as asymmetric omphacite pressure shadows around augite or diopside porphyroclasts, micro-faulted porphyroclasts, sigma-type porphyroclast systems or shear bands marked by glaucophane (Fig. 9). These criteria indicate that ductile shear was non-coaxial, took place under blueschist to eclogite facies conditions and that the shear sense was top-to-the-west.

Conversely, in thin sections parallel to the N80°E lineation, criteria such as asymmetric pressure shadows of tremolite + clinochlore + clinozoisite around augite or diopside porphyroclasts, micro-faulted porphyroclasts, sigma-type

porphyroclast systems or shear bands (Fig. 10) indicate that the ductile shear was non-coaxial, occurred under greenschist facies conditions, and that the shear sense is top-to-the-east. Most importantly, Fig. 10 shows greenschist facies mineral assemblage (tremolite + clinochlore + clinozoisite) along shear bands that offset glaucophane-marked foliation, indicating that the east-verging shear post-dates the blueschist to eclogite facies shear, that is, the west-verging shear.

5.2. Pseudotachylyte veins

In rare instances, ductile deformed pre-mylonitization pseudotachylyte veins contain clasts flanked with asymmetric omphacite overgrowths indicating non-coaxial shear with top-to-the-west senses (Fig. 9D). Such observations agree with the kinematics recorded in the host mylonitic metagabbro.

Four hand samples from either the mylonitic sole or from secondary shear zones indicate that the sense of displacement associated with the formation of amphibole-bearing pseudotachylyte veins is top-to-the-east or top-to-the-northeast (Fig. 11). Despite the small number of samples, the sense of displacement associated with the formation of amphibole-bearing pseudotachylyte veins is tentatively supposed to be top-to-the-east or top-to-the-northeast. Such a kinematics is in accordance with the top-to-the-east sense of shear in the mylonitic gabbro under greenschist facies conditions

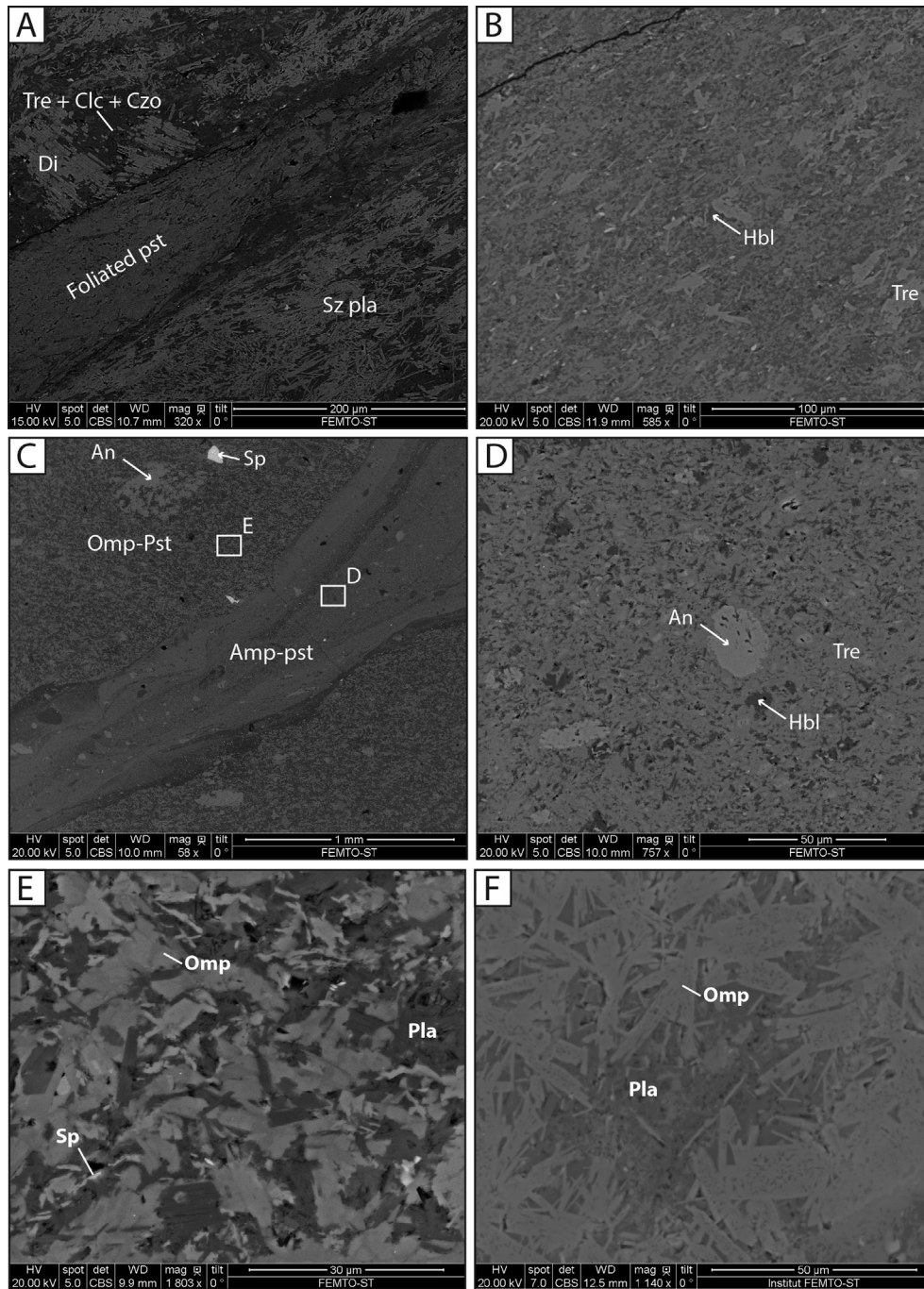


Fig. 8. Scanning electron microscope (SEM) images of metagabbro pseudotachylyte. A: pre-mylonitization fault vein in mylonitic metagabbro. B: post-mylonitization fault vein in mylonitic metagabbro. C: amphibole-bearing pseudotachylyte vein intruded across an omphacite-bearing pseudotachylyte vein. D: Close view of the amphibole-bearing pseudotachylyte vein showing a clast of anorthite and tremolite and hornblende microlites. E: Close view of omphacite-bearing pseudotachylyte vein with microlites of omphacite and plagioclase. F: Skeletal texture of omphacite microlites in an omphacite-bearing pseudotachylyte vein. Abbreviations: Amp: amphibole, An: anorthite, Clc: clinocllore, Czo: clinzoisite, Di: diopside, Hbl: hornblende, Pla: plagioclase, pst: pseudotachylyte, Omp: omphacite, Sp: serpentine, Sz pla: sericitized plagioclase, Tre: tremolite.

(Fig. 10).

6. Discussion

6.1. Chronology of deformation in the mafic unit DZs and correlation with the upper part of the ultramafic unit

The succession of deformation episodes recorded in the damage zones (DZs) flanking ϕ_2 is summarized in Fig. 12. The oldest

recorded event D1 consists of a west-directed ductile shear under greenschist facies conditions at the base of the mafic unit and locally within the unit (secondary shear zones). This ductile shear is considered responsible for the formation of the foliation and the N120°E lineation. D1 is followed by brittle event D2 responsible for the formation, in the mylonitic sole, of pseudotachylyte veins under blueschist to eclogite facies conditions. Likely contemporaneous with D2 (though difficult to ascertain) is the formation of pseudotachylyte under similar blueschist to eclogite facies conditions in

Table 1
Average composition of microlites and clasts in pseudotachylyte veins from the equant metagabbro, mafic unit.

wt.% analysis	Mylonitized pseudotachylytes			Omphacite-bearing pseudotachylyte					Amphibole-bearing pseudotachylytes			
	Clast	Pressure shadow	Matrix	Clast	Clast	Microlite	Microlite	Microlite	Clast	Microlite	Microlite	Bulk matrix
	Anorthite	Omphacite	Albite	Augite	Anorthite	Omphacite	Augite	Sphene	Anorthite	Tremolite	Mg-Hornblende	
SiO ₂	35,59	43,1	68,58	53,67	45,66	43,1	52,21	20,21	42,74	54,52	54,65	43,18
MgO	0,02	15,35	0,61	15,83	0,12	15,35	19,32	0,42	0,46	19,72	16,63	6,33
FeO	2,57	8,03	0,28	3,98	1,13	8,03	6	0,37	1,91	5,01	5,24	2,59
Al ₂ O ₃	31,31	16,05	19,22	12,62	30,13	16,05	6,88	1,04	30,38	5,3	9,1	31,85
Na ₂ O	0,09	3,2	11,01	2,25	2,66	3,2	1,44	0,11	1,25	1,37	1,91	5,58
CaO	24,02	11,19	0,46	9,48	19,29	11,19	12,38	18,09	21,1	11,75	10,28	0,8
K ₂ O	0,01	0,05	0	0,07	0	0,05	0,05	0	0	0	0,06	0,2
MnO	0,18	0,29	0	0,05	0	0,29	0,1	0	0,03	0,13	0,09	0,04
TiO ₂	0,04	0,87	0	0,06	0,02	0,87	0,05	59,46	0	0,05	0	0
Cr ₂ O ₃	0	0,08	0	0,03	0,01	0,08	0,05	0,26	0,01	0,03	0	0,04
NiO	0	0,15	0,02	0	0,03	0,15	0,12	0,01	0,03	0	0	0
Total	97,84	98,36	100,17	98,02	99,05	98,36	98,61	9,98	97,91	97,86	97,96	90,62
Est. H ₂ O	2,16	1,64		1,98	0,95	1,64	1,39	0,02	2,09	2,14	4,51	9,38

the equant metagabbro. No kinematics can be related to D2 pseudotachylytes. D3 corresponds to a westward-directed (N120°E) ductile shear under continuing blueschist to eclogite facies conditions. This shear is also responsible for the mylonitization of pseudotachylyte veins formed during D2. The D1 to D3 succession is considered to have taken place within the subducting lithosphere of the Piemonte-Liguria Ocean in Cretaceous to Eocene times (Fig. 13).

D4 corresponds to a N80°E-directed shear under greenschist facies conditions (see Fig. 12). D5 is the second faulting event at the origin of the formation, in greenschist facies conditions, of pseudotachylyte veins in the mylonitic sole as well as in the equant metagabbro. Whatever the host rock, these pseudotachylyte veins were not subsequently ductilely deformed. No kinematics can be related to D5 pseudotachylytes. Eastward vergence of D4 and the retrograde (greenschist facies) conditions prevailing during D4 and D5 suggest that these two events took place during late-to post-collision extensional collapse of the mountain belt in Oligocene times, as observed in other Corsican Alpine units by Jolivet et al. (1990, 1991), Fournier et al. (1991), Daniel et al. (1995), Lahondère (1996) and Molli and Malavieille (2011). D4 and D5 are considered as distinct from the early, pre-collisional, subduction history.

Below φ_2 , the ultramafic unit shows either brittle structures (pseudotachylyte) in peridotite of A or B type DZs, or ductile structures (foliation and faint lineation) in serpentinite or meta-sedimentary rocks of C type DZs. Magott et al. (2016) showed that pseudotachylyte in the peridotite formed during west-directed reverse faulting. Such a kinematics, confirmed by Ferré et al. (2016), is compatible with events D1 and D3, given the fact that the peridotite likely remains brittle even in conditions under which gabbro is ductile. Conversely, since serpentine can shift to a 'ductile' (distributed) behavior as early as D1 (greenschist facies conditions), ductile deformation of the serpentinite can therefore have lasted from D1 through D2 until D3. The kinematics of the deformation of the serpentinite is unknown, due to the lack of shear sense criteria. What happened in the ultramafic unit during D4 and D5 remains undetermined, due to the lack of kinematic or metamorphic constraints that would allow correlations between the two units.

The D1 to D5 succession mixes aseismic plastic deformation (odd-numbered events) and brittle co-seismic deformation (even-numbered events). Such a mixing is particularly obvious in the mylonitic sole and associated secondary shear zones where both pre- and post-mylonitization pseudotachylyte veins are preserved. Similar co-occurrences of aseismic plastic/seismic brittle structures are reported from various settings (Sibson, 1980; Passchier, 1982;

Hobbs et al., 1986; McNulty, 1995; Lin et al., 2003; Zechmeister et al., 2007). Various mechanisms were proposed to account for this co-occurrence, among which the most often invoked are propagation of the seismic rupture downwards through the plastosphere (e.g., Sibson, 1980) and thermal shear instabilities (e.g., Hobbs et al., 1986). Given the subduction zone setting of the study area, the coexistence of brittle and ductile structures along φ_2 could reflect oscillations of the Wadati-Benioff surface-parallel isotherms near the brittle/plastic boundary zone, as advocated by Magott et al. (2016).

6.2. Geodynamic setting for the deformation history of the mafic unit/ultramafic unit interface

The succession of two ductile deformation episodes consisting of an early west-directed shear under blueschist to eclogite facies conditions and a late east-directed shear under greenschist facies conditions has already been described in the tectonic units surrounding the Cima di Gratera nappe by many authors. Some authors put emphasis on the early prograde west-directed shear as a consequence of the east-dipping subduction of the Piemonte-Liguria Ocean in Cretaceous to Eocene times (e.g., Mattauer and Proust, 1976; Mattauer et al., 1977, 1981) while other authors focused their attention on the late retrograde top-to-the-east shear and its link with late-to post-collision extension in Oligocene times (Jolivet et al., 1990, 1991; Fournier et al., 1991; Daniel et al., 1995; Lahondère, 1996; Brunet et al., 2000; Molli and Malavieille, 2011).

The D1 to D3 succession of events in the mafic unit is compatible with top-to-the-west reverse faulting (pseudotachylyte) in the ultramafic unit. In the mafic unit and supposedly in the ultramafic unit, metamorphic conditions increased from greenschist facies to eclogite facies conditions between D1 and D3. The D1 to D3 succession is interpreted as resulting from non-coaxial reverse faulting/ductile shear in the descending slab at depths at which P/T conditions are between greenschist facies to eclogite facies conditions. The highest metamorphic conditions (omphacite) correspond to depths between 60 and 90 km, assuming a mean rock density of 3000 kg/m³ and lithostatic equilibrium. The alternating distributed crystal plastic (aseismic)/localized brittle (seismic) deformation conditions in the mafic unit can reflect temporal variations of the temperature along the Wadati-Benioff zone and corresponding depth oscillations of the brittle-plastic transition, as discussed above (Section 6.1). Concurrently, in the underlying ultramafic unit, brittle (seismic) deformation took place in peridotite while distributed brittle deformation (cataclastic flow) prevailed in

Top-to-the-west shear criteria

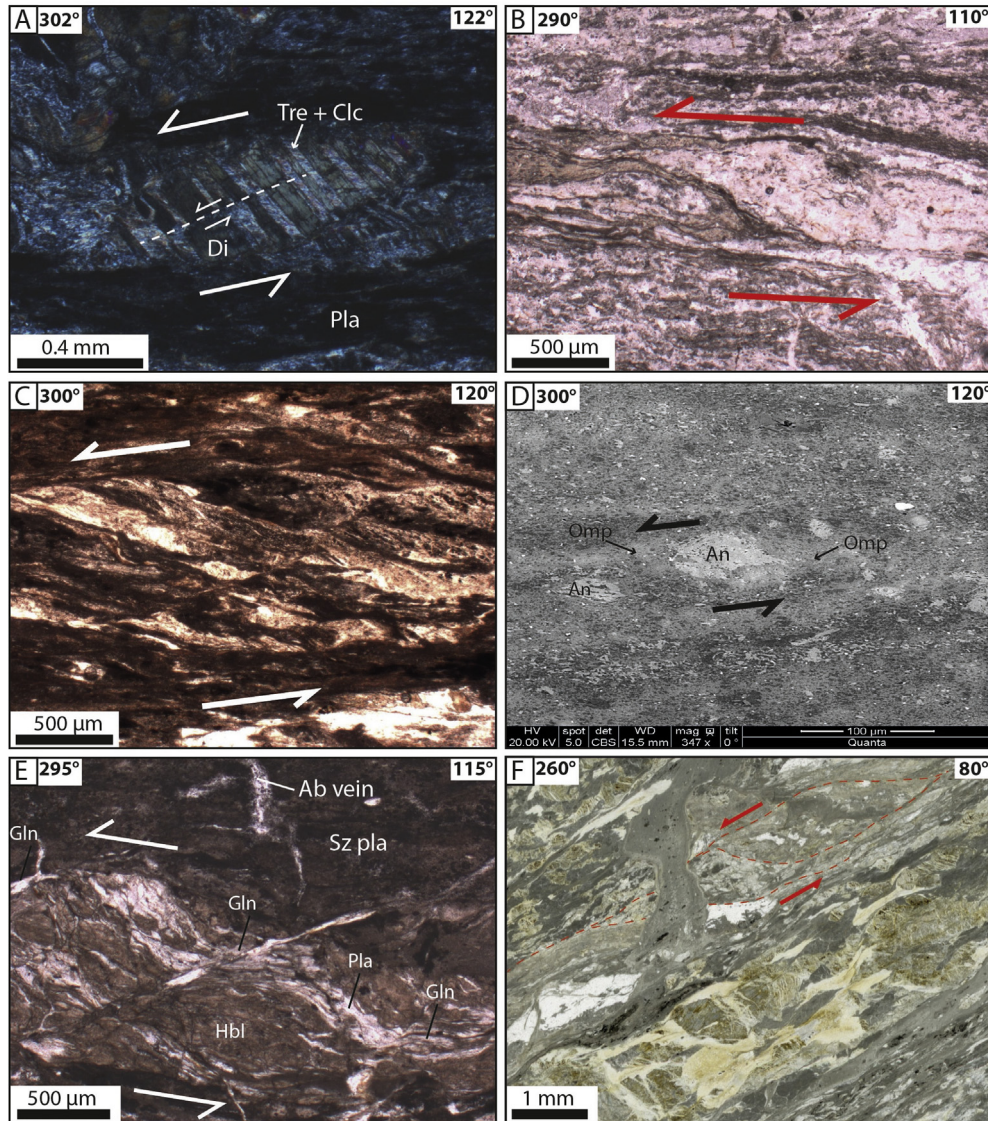


Fig. 9. Photomicrographs (A, B, C, E and F) and SEM images (D) of top-to-the-west greenschist to blueschist facies ductile shear sense criteria in metagabbro or in metagabbro-hosted pseudotachylyte. Localities refer to Fig. 1. A: diopside porphyroclast crossed by a normal microfault and flanked by asymmetric tails of fibrous tremolite + clinchlore (metagabbro, locality E). B: plagioclase porphyroclast flanked by asymmetric tails of glaucophane (metagabbro, locality B). C: shear bands offsetting the foliation of the mylonitic metagabbro (locality D). D: elongated albite 'survivor' clast flanked by asymmetric tails of omphacite (pre-mylonitization pseudotachylyte vein, locality E). E: shear bands marked by glaucophane and deflecting the foliation of a mylonitic metagabbro (locality B). F: deformed sericitized plagioclase sigmoidal porphyroclast. Note that the porphyroclast is crossed by a (post-mylonitization) pseudotachylyte injection vein (mylonitic metagabbro, locality D). Same abbreviations as for Fig. 8. Ab: albite, Gln: glaucophane.

serpentinites. A preliminary dating of an omphacite-bearing pseudotachylyte vein crossing an equant metagabbro by the $^{40}\text{Ar}/^{39}\text{Ar}$ method has yielded a 54 ± 10 Ma age. The large uncertainty likely reflects argon excess in the analyzed sample. However, despite the uncertainty, this preliminary age is in agreement with the 60–55 to 34 Ma ages of the HP/LT metamorphism obtained in units around the Cima di Gratera nappe (Vitale-Brovarone and Herwartz, 2013, and references therein).

6.3. Significance of the lateral transition from pseudotachylyte-bearing to pseudotachylyte-free DZs

Detailed mapping of the walls of φ_2 (Figs. 1 and 3) shows that A type DZs are characterized by pseudotachylyte veins on either side of φ_2 and by the lack of mineralized veins. Conversely, C type DZs lack pseudotachylyte and show mineralized veins along with serpentinization of φ_2 footwall where the latter consists of mantle rocks (not sedimentary rock lenses). With a lesser amount of pseudotachylyte and a larger amount of mineralized veins than for

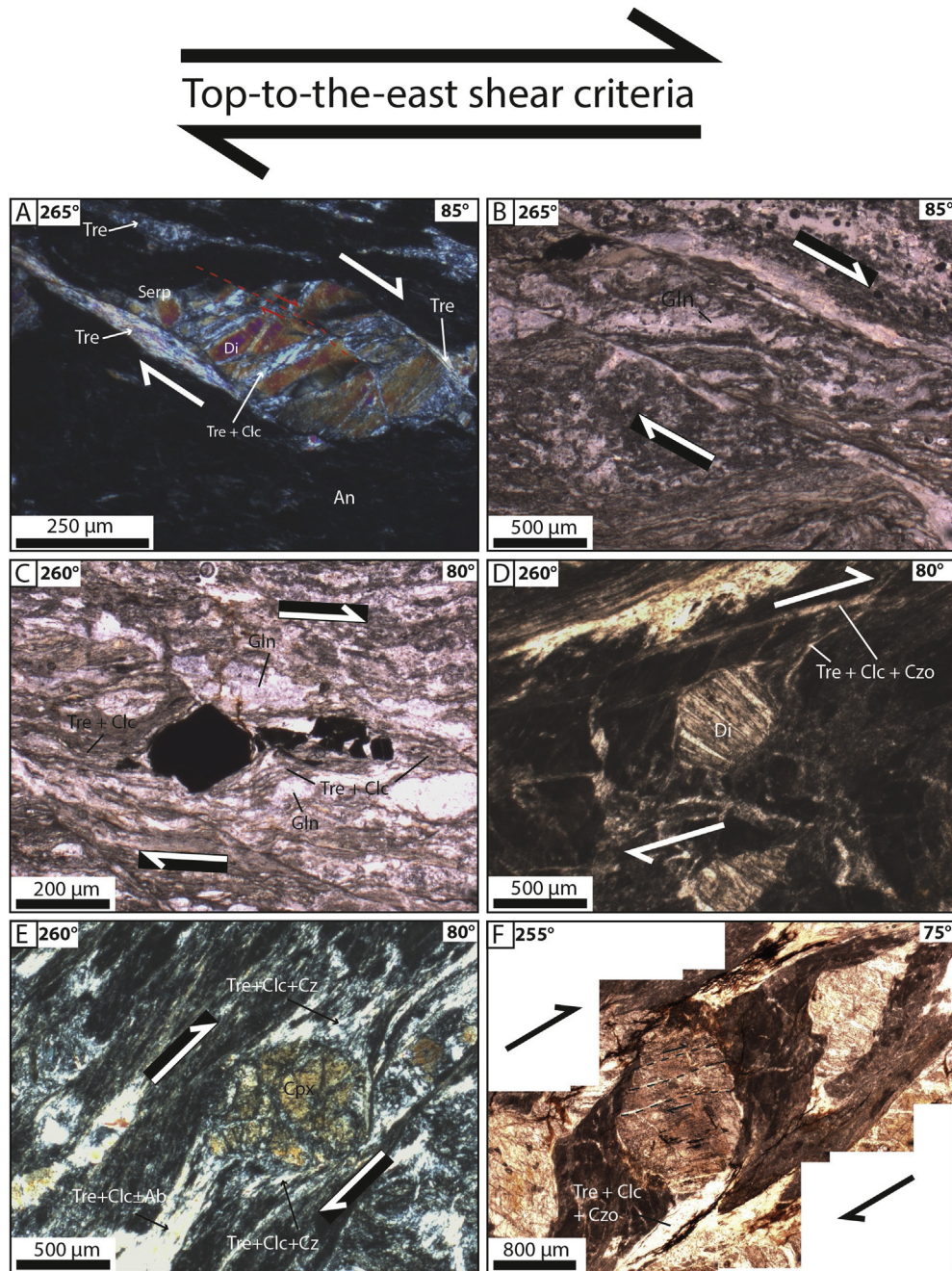


Fig. 10. Photomicrographs of top-to-the-east greenschist facies ductile shear sense criteria in mylonitic metagabbro. Localities refer to Fig. 1. A: sigmoidal diopside porphyroblast flanked with tremolite overgrowths (locality E). B: shear bands outlined by tremolite + clinocllore + clinozoisite and offsetting glaucophane-marked foliation (locality B). C: opaque minerals flanked by asymmetric tremolite + clinocllore overgrowths (locality A). D: diopside porphyroblast flanked by tremolite + clinocllore + clinozoisite overgrowths (locality D). E: clinopyroxene with recrystallized tails and tremolite + clinocllore + clinozoisite overgrowths (locality D). F: diopside porphyroblast crossed by reverse microfaults and flanked by tremolite + clinocllore + clinozoisite overgrowths (locality D). Same abbreviations as for Fig. 8. Czo: clinozoisite, Serp: serpentine.

A type DZ, B type DZs are considered as representing a transitional type between A and C type DZs.

These observations suggest that interfaces between peridotite and gabbro in A type DZs were preferential sites for frictional melting, along or near the contact (Fig. 14). Though it is not possible to estimate the amount of pseudotachlyte generated and the number of earthquakes that could have led to the production of this amount, A type DZ interfaces may be regarded as patches where the co-seismic displacements were larger than along the surrounding B or C type DZs. The larger amount of melting can result from larger

amounts of strain accumulated in A type DZs due to higher mechanical strength of peridotite or to larger coefficients of friction of the gabbro-peridotite interface (e.g., Del Gaudio et al., 2009; Niemeijer et al., 2011). Conversely, the foliated serpentinite or the metasediments of the other end-member interface (C type DZ) are intrinsically weaker than the massive peridotite, and the coefficients of friction of serpentinite-gabbro or metasediment-gabbro contact surfaces are likely weaker than the gabbro-peridotite one (Reinen et al., 1991, 1994; Moore et al., 1997; Hirose and Bystricky, 2007; Kohli et al., 2011; Sone et al., 2012;

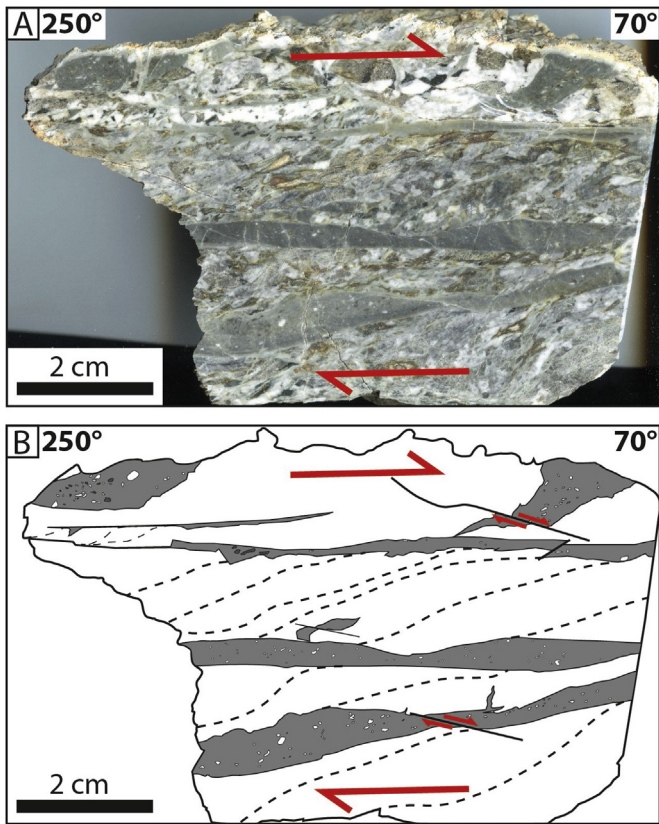


Fig. 11. Polished metagabbro hand sample showing top-to-the-east offset of the foliation of a secondary shear zone by amphibole-bearing pseudotachylyte fault veins (locality C, Fig. 1). The offset of fault veins by Riedel-like microfaults is also consistent with the top-to-the east sense of displacement.

Proctor et al., 2014; Brantut et al., 2016). Given the strength and/or the friction contrasts, it is likely that the gabbro-peridotite interfaces can accumulate more interseismic strain than the serpentinite-gabbro or sediment-gabbro interfaces, thus experiencing larger co-seismic displacements during ruptures.

In addition to contrasted peridotite and serpentinite mechanical properties, the likely presence of over-pressurized fluids along ϕ_2 (as suggested by mineralized veins, especially the flat-lying ones) may also have played a role in the weakening of the contact along B or C type DZs. Such over-pressurized fluids may lower the strength of the interface, allowing less strain accumulation and therefore less release of energy during earthquakes. Ultimately, over-pressurized fluids may prevent the serpentinite-gabbro contact surfaces from locking, allowing creep and rendering seismic ruptures unlikely or of small magnitudes.

Assuming that the gabbro-peridotite contacts (A type DZs) correspond to some extent to seismological asperities, it is then necessary to compare the sizes of the two types of heterogeneities. In the study area, the exposed widths of A type DZs are between 0.5 and 1 km (Fig. 1). Assuming that these exposed widths are the largest expected and that the shape of the heterogeneity is close to a square or a circle, the area of the A type contacts is less than about 1 km². Such a surface is significantly smaller than most asperities reported from subduction interfaces. However, several authors describe asperities whose areas are of the order of 1 km² or even less (Bakun and McEvilly, 1984; Nadeau et al., 1995; Igarashi et al., 2003; Seno, 2003). Geological asperities suspected in the study area may include a part of the surrounding B type contacts, increasing the actual sizes. The 1 km² value is clearly a conservative estimate.

The interpretation proposed here to account for the uneven distribution of fault rocks and the related damage zone types along the ϕ_2 fault presents some analogy with the so-called ‘ancient seismogenic coupling zone’ described by Bachmann et al. (2009) in the central Alps. Even if the location of the two fault zones differ (inside the subducting slab in the Corsican case vs. along the plate interface in the central Alps case), both interfaces are characterized by patches of large co-seismic slip (asperities) surrounded by creeping zones. Another major difference between the two structures lies in the role played by fluids, which is not surprising given the location difference mentioned above: fluids played a key role in the central Alps example and a minor role in the Corsican example. More broadly, a similar heterogeneous distribution of co-seismic slip suggested by pseudotachylyte-rich patches surrounded by pseudotachylyte-free domains can be suspected along seismic faults in extensional contexts such as the Basin and Range detachments (John, 1987; John and Foster, 1993) or the West Iberia margin (Manatschal et al., 2001) where the products of frictional melt were recovered, or such as oceanic core complexes, but frictional melting along these structures has still to be proven (Schroeder and John, 2004; Miranda and John, 2010).

7. Conclusion

The structural analysis of the ϕ_2 tectonic contact and relevant damage zones in the Cima di Gratera nappe leads to the following results.

- (1) The Cima di Gratera nappe contains a major fault which recorded a complex succession of five brittle/ductile deformation events. D1 to D3 deformation events are consistent with a prograde ductile/brittle deformation under high-grade (greenschist to eclogite facies) conditions during the subduction of the Piemonte-Liguria oceanic lithosphere. D4 and D5 stages are related to retrograde metamorphism and deformation in association to the syn-to post-orogenic extension.
- (2) The major fault preserved in the Cima di Gratera nappe is characterized by three types of damage zones. One end-member (A type DZ) corresponds to gabbro-peridotite contacts and is characterized by numerous pseudotachylyte veins on either side of the fault. The other end-member (C type DZ) is observed where gabbro is in contact with foliated serpentinite or with meta-sedimentary rocks. It is characterized by the absence of pseudotachylyte and by the presence of discrete mineralized veins. The B type DZ is intermediate between the two end-members.
- (3) Regarding A or B type DZs, in the localities where the peridotite is partly serpentinitized, formation of pseudotachylyte clearly predates serpentinitization.
- (4) The abundance of pseudotachylyte veins along or near A type DZs suggests that gabbro-peridotite contacts released large amounts of co-seismic slip during a likely large number of events. Conversely, the paucity of pseudotachylyte along or near C type DZs suggests that gabbro-serpentinite or gabbro-metasedimentary rocks did not release significant amounts of co-seismic slip, possibly because their incapacity to accumulate large inter-seismic strain (Fig. 14). This incapacity likely results from the poor ability (weak mechanical strength) of footwall serpentinite or sedimentary rocks to store significant amounts of elastic energy and their propensity to deform aseismically, either plastically or through distributed cataclasis.
- (5) As suggested by mineralized veins, fluid flow possibly played a role in the weakening of C and to a lesser extent of B type

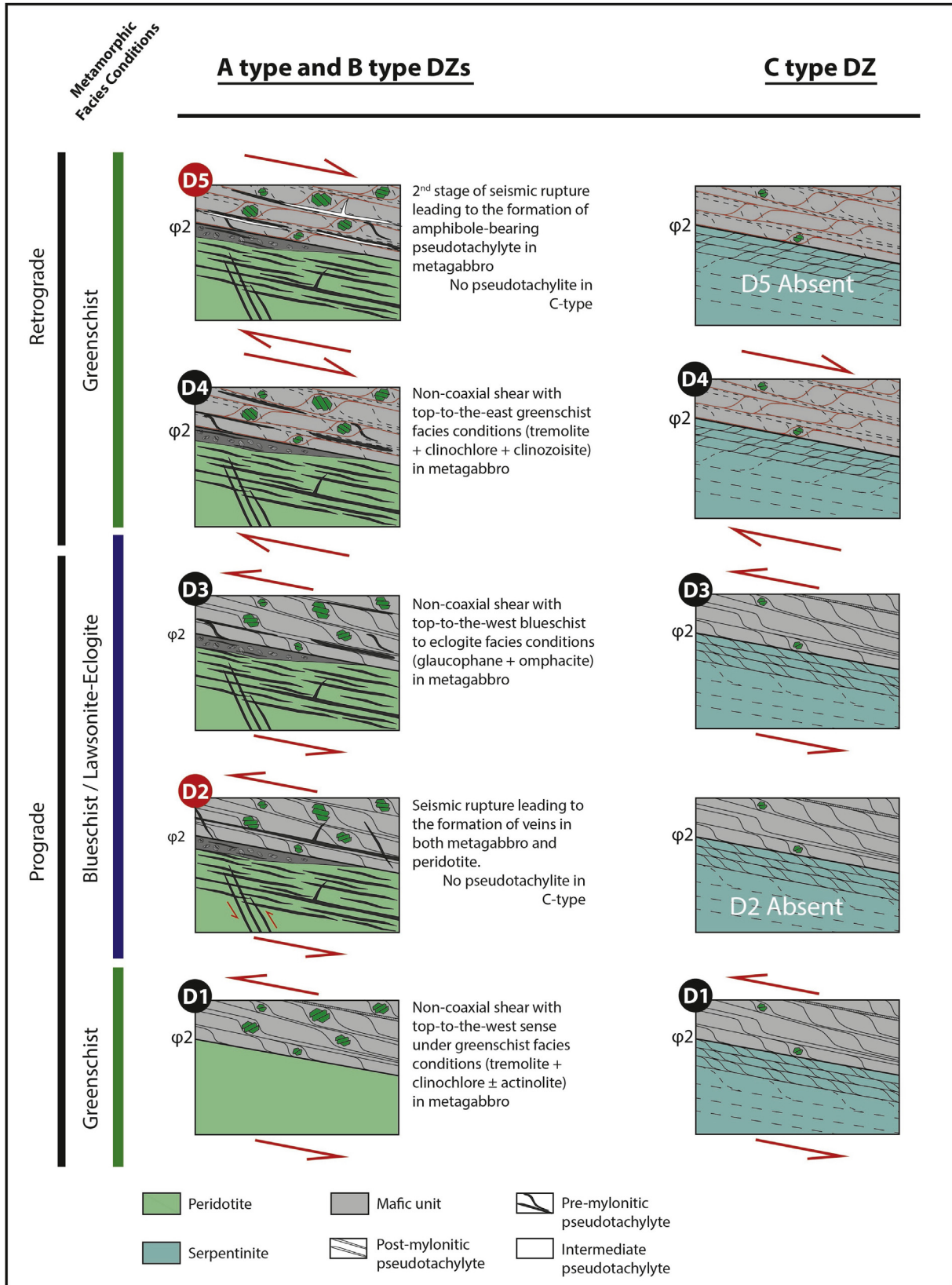


Fig. 12. Synthesis of the succession of deformation events (D1 to D5) recorded in the damage zones (DZs) flanking ϕ_2 . The depicted breccia stands for the *intermediate pseudotachylite* characterizing A type DZ. Deformation events D2 and D5, which consist of pseudotachylite formation (seismic faulting), are labelled in red. (For interpretation of the references to colour in this figure legend, the reader is referred to the web version of this article.)

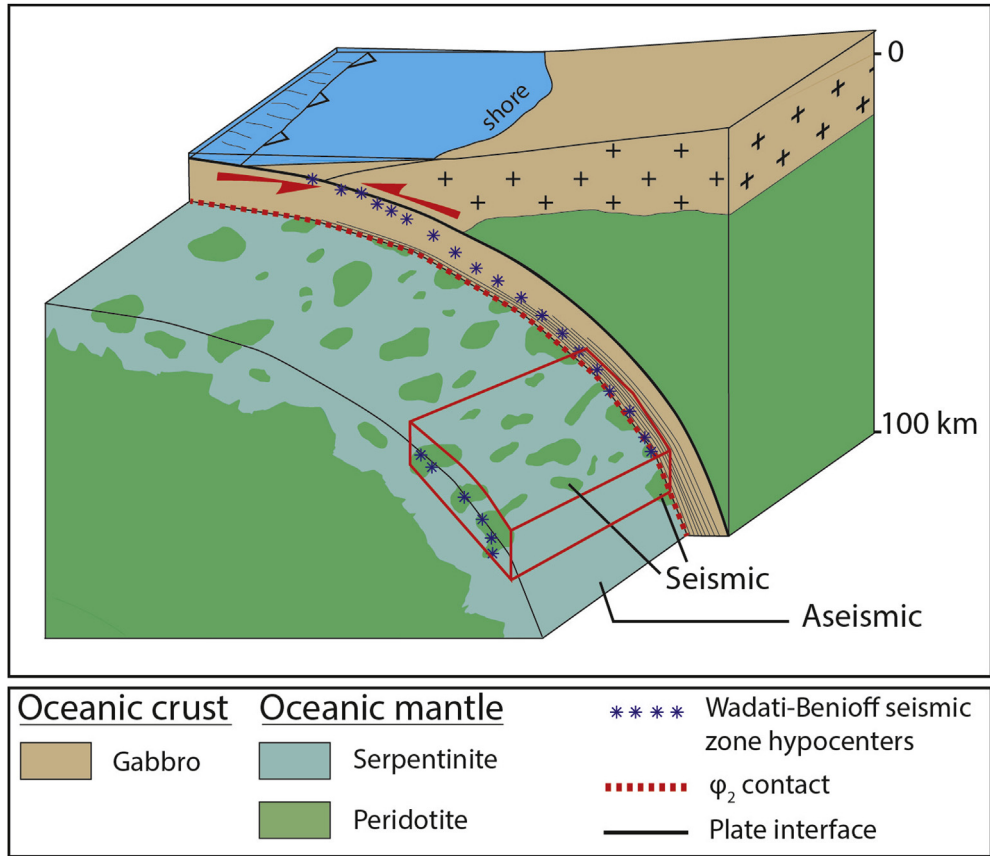


Fig. 13. Schematic block diagram (scale is approximate) showing the supposed geodynamical framework of the D1 to D3 deformation events along or near ϕ_2 (boxed volume). Above ϕ_2 , the metagabbro is deformed either in a brittle mode (pseudotachylite) or in a ductile mode (mylonite). Below ϕ_2 , fresh peridotite is deformed in a brittle mode while serpentinite is deformed in a 'ductile' (distributed cataclastic) mode.

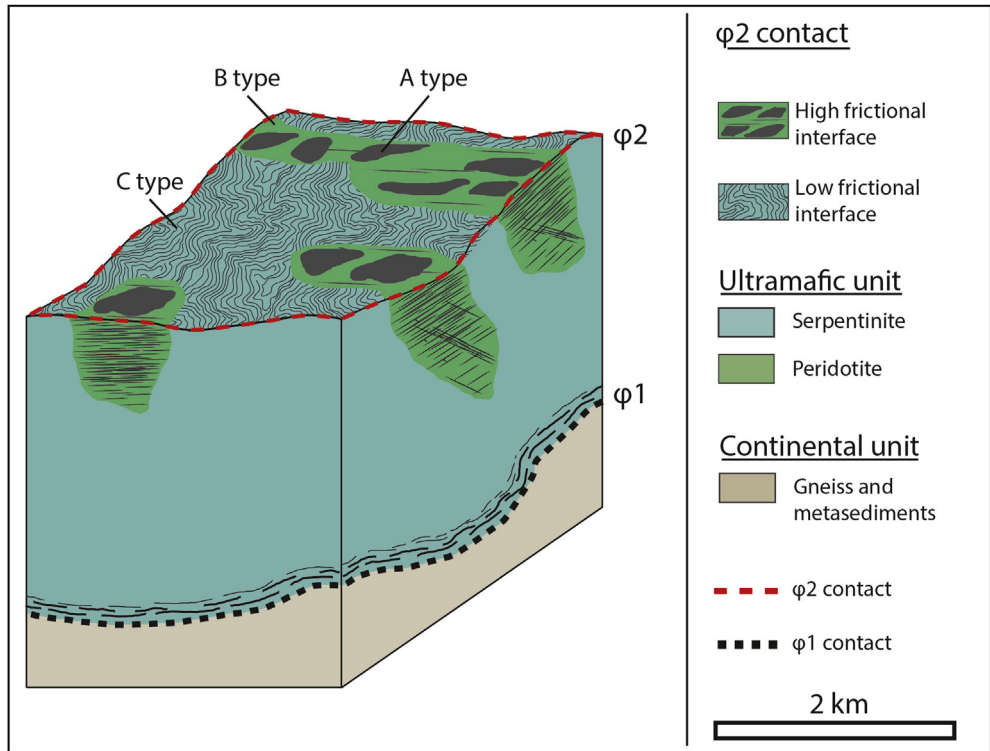


Fig. 14. Block diagram showing the Cima di Gratera ultramafic unit after removal of the mafic unit. The uppermost surface of the unit consists either of foliated serpentinite or massive peridotite. The coefficient of friction of the gabbro-serpentinite contact is weak, allowing distributed slip without significant melting. The coefficient of friction of the gabbro-peridotite contact is higher, leading to seismic ruptures with significant frictional melting.

contacts through a more intense serpentinization of the peridotite.

The coexistence along fault zones of pseudotachylyte-rich patches surrounded by pseudotachylyte-poor or pseudotachylyte-free domains is reminiscent of the asperity model proposed for seismic faults in various types of tectonic contexts. The Corsican example described here is however original since it may correspond to a fault zone which was active inside a subducting slab and not along the interface between two plates in a subduction setting. Pseudotachylyte appears as a key tool to recognize and to map asperity-like heterogeneities in major fault zones, whatever the tectonic context.

Acknowledgments

This work was funded by the CNRS-INSU TelluS-ALEAS program. Scanning electron microscopy was supported by the RENATECH network. We acknowledge stimulating discussions with Philippe Agard and Claudio Rosenberg. Patrick Monié is thanked for preliminary attempts of pseudotachylyte dating. Constructive reviews by Eric Ferré and Giancarlo Molli helped clarifying several key points.

References

- Aki, K., 1979. Characterization of barriers on an earthquake fault. *J. Geophys. Res. (Solid Earth)* 84, 6140–6148.
- Andersen, T.B., Austrheim, H., 2006. Fossil earthquakes recorded by pseudotachylytes in mantle peridotites from the Alpine subduction complex of Corsica. *Earth Planet. Sci. Lett.* 242, 58–72.
- Andersen, T.B., Mair, K., Austrheim, H., Podladchikov, Y.Y., Vrijmoed, J.C., 2008. Stress release in exhumed intermediate and deep earthquakes determined from ultramafic pseudotachylyte. *Geology* 36, 995–998.
- Andersen, T.B., Austrheim, H., Deseta, N., Silkose, P., Ashwal, L.D., 2014. Large subduction earthquakes along the fossil Moho in Alpine Corsica. *Geology* 42, 395–398. <http://dx.doi.org/10.1130/G35345.1>
- Astiz, L., Lay, T., Kanamori, H., 1988. Large intermediate-depth earthquakes and the subduction process. *Phys. Earth Planet. Inter.* 53, 80–166.
- Austrheim, H., Andersen, T.B., 2004. Pseudotachylytes from Corsica: fossil earthquakes from a subduction complex. *Terra Nova* 16, 193–197 doi: 10/1111/j.1365-3121.2004.00551.x.
- Austrheim, H., Boundy, T.M., 1994. Pseudotachylytes generated during seismic faulting and eclogitization of the deep crust. *Science* 265, 82–83.
- Bachmann, R., Oncken, O., Glodny, J., Seifert, W., Georgieva, V., Sudo, M., 2009. Exposed plate interface in the European Alps reveals fabric styles and gradients related to an ancient seismogenic coupling zone. *J. Geophys. Res. (Solid Earth)* 114, B05402. <http://dx.doi.org/10.1029/2008JB005927>.
- Bakun, W.H., McEvilly, T.V., 1984. Recurrence models and Parkfield, California, earthquakes. *J. Geophys. Res. (Solid Earth)* 89, 3051–3058.
- Brantut, N., Passetegue, F.X., Deldicque, D., Rouzaud, J.N., Schubnel, A., 2016. Dynamic weakening and amorphization in serpentinite during laboratory earthquakes. *Geology* 44, 607–610.
- Brunet, C., Monié, P., Jolivet, L., Cadet, J.P., 2000. Migration of compression and extension in the Tyrrhenian Sea, insights from ⁴⁰Ar/³⁹Ar ages on micas along a transect from Corsica to Tuscany. *Tectonophysics* 321, 127–155.
- Bürgmann, R., Kogan, M.G., Steblow, G.M., Hiley, G., Levin, V.E., Apel, E., 2005. Interseismic coupling and asperity distribution along the Kamchatka subduction zone. *J. Geophys. Res. (Solid Earth)* 110, B07405. <http://dx.doi.org/10.1029/2005JB003648>.
- Daniel, J.M., Jolivet, L., Goffé, B., Poinssot, C., 1995. Crustal-scale strain partitioning: footwall deformation below the Alpine Oligo-Miocene detachment of Corsica. *J. Struct. Geol.* 18, 41–59.
- Das, S., Aki, K., 1977. Fault plane with barriers: a versatile earthquake model. *J. Geophys. Res. (Solid Earth)* 82, 5658–5670.
- Del Gaudio, P., Di Toro, G., Han, R., Hirose, T., Nielsen, S., Shimamoto, T., Cavallo, A., 2009. Frictional melting of peridotite and seismic slip. *J. Geophys. Res. (Solid Earth)* 114, B06306. <http://dx.doi.org/10.1029/2008JB005990>.
- Deseta, N., Andersen, T.B., Ashwal, L.D., 2014a. A weakening mechanism for intermediate-depth seismicity? Detailed petrographic and microstructural observation from blueschist facies pseudotachylytes, Cape Corse, Corsica. *Tectonophysics* 610, 138–149.
- Deseta, N., Ashwal, L.D., Andersen, T.B., 2014b. Initiating intermediate-depth earthquakes: insights from a HP-LT ophiolite from Corsica. *Lithos* 206, 127–146.
- Durand-Delga, M., Rossi, P., 2002. About the ligurian-piemontese jurassic ocean on the transect Corsica-Apennines. *Comptes Rendus Géosci.* 334, 227–228.
- Escartin, J., Hirth, G., Evans, B., 1997. Nondilatant brittle deformation of serpentinites: implications for Mohr-Coulomb theory and the strength of faults. *J. Geophys. Res. (Solid Earth)* 102, 2897–2913.
- Faure, M., Malavieille, J., 1981. Etude structurale d'un cisaillement ductile: le charriage ophiolitique corse dans la région de Bastia. *Bull. Soc. Géol. Fr.* 23, 335–343.
- Ferré, E.C., Chou, Y.M., Kuo, R.L., Yeh, E.C., Leibovitz, N.R., Meado, A.L., Campbell, L., Geissman, J.W., 2016. Deciphering viscous flow of frictional melts with the mini-AMS method. *J. Struct. Geol.* 90, 15–26.
- Fournier, M., Jolivet, L., Goffé, B., Dubois, R., 1991. Alpine Corsica metamorphic core complex. *Tectonics* 10, 1173–1186.
- Frohlich, C., 2006. *Deep Earthquakes*. Cambridge University Press, p. 573.
- Guerrera, F., Martin-Algarra, A., Perrone, V., 1993. Late Oligocene-Miocene syn-/late-orogenic successions in western and central Mediterranean chains from the Betic Cordillera to the Southern Apennines. *Terra Nova* 5, 525–544.
- Hasegawa, A., Uchida, N., Igarashi, T., Matsuzawa, T., Okada, T., Miura, S., Suwa, Y., 2007. Asperities and quasi-static slips on the subducting plate boundary east of Tohoku, Northeast Japan. In: Dixon, T.H., Moore, J.C. (Eds.), *The Seismogenic Zone of Subduction Thrust Faults*. Princeton University Press, pp. 451–475.
- Hirose, T., Bystricky, M., 2007. Extreme dynamic weakening of faults during dehydration by coseismic shear heating. *Geophys. Res. Lett.* 34, L14311. <http://dx.doi.org/10.1029/2007GL030049>.
- Hobbs, B.E., Ord, A., Teyssier, C., 1986. Earthquakes in the ductile regime? *Pure Appl. Geophys.* 124, 309–336.
- Igarashi, T., Matsuzawa, T., Hasegawa, A., 2003. Repeating earthquakes and interplate aseismic slip in the northeastern Japan subduction zone. *J. Geophys. Res. (Solid Earth)* 108. <http://dx.doi.org/10.1029/2002JB001920>.
- John, B.E., 1987. Geometry and evolution of a mid-crustal extensional fault system: Chemehuevi Mountains, southeastern California. *Geol. Soc.* 28, 313–335. London, Special Publications.
- John, B.E., Foster, D.A., 1993. Structural and thermal constraints on the initiation angle of detachment faulting in the southern Basin and Range: the Chemehuevi Mountains case study. *Geol. Soc. Am. Bull.* 105, 1091–1108.
- John, T., Medvedev, S., Rüpke, L.H., Andersen, T.B., Podladchikov, Y.Y., Austrheim, H., 2009. Generation of intermediate-depth earthquakes by self-localizing thermal runaway. *Nat. Geosci.* 2, 137–140. <http://dx.doi.org/10.1038/NGEO419>.
- John, T., Schenk, V., 2006. Interrelations between intermediate-depth earthquakes and fluid flow within subducting oceanic plates: constraints from eclogite facies pseudotachylytes. *Geology* 34, 557–560.
- Jolivet, L., Dubois, R., Fournier, M., Goffé, B., Michard, A., Jourdan, C., 1990. Ductile extension in Alpine Corsica. *Geology* 18, 1007–1010.
- Jolivet, L., Daniel, J.M., Fournier, M., 1991. Geometry and kinematics of extension in Alpine Corsica. *Earth Planet. Sci. Lett.* 104, 278–291.
- Kanamori, H., Stewart, G.S., 1978. Seismological aspects of the Guatemala earthquake of February 4, 1976. *J. Geophys. Res. (Solid Earth)* 83, 3427–3434.
- Kohli, A.H., Goldsby, D.G., Hirth, G., Tullis, T., 2011. Flash weakening of serpentinite at near-seismic slip rates. *J. Geophys. Res. (Solid Earth)* 116, B03202. <http://dx.doi.org/10.1029/2010JB007833>.
- Lagabrielle, Y., Vitale-Brovarone, A., Ildefonse, B., 2015. Fossil oceanic core complexes recognized in the blueschist metaophiolites of western Alps and Corsica. *Earth-Sci. Rev.* 141, 1–26.
- Lahondère, D., 1996. Les schistes bleus et les éclogites à lawsonite des unités continentales et océaniques de la Corse alpine. *Doc. Du BRGM* 240, 294. Orléans.
- Lay, T., Kanamori, H., 1981. An asperity model for large earthquake sequences. In: Simpson, D., Richard, P. (Eds.), *Earthquake Prediction, an International Review*, vol. 4, pp. 579–592. AGU Monograph Maurice Ewing Series.
- Lay, T., Kanamori, H., Ruff, L., 1982. The asperity model and the nature of large subduction zone earthquakes. *Earthq. Predict. Res.* 1, 3–71.
- Legrand, D., Tassara, A., Morales, D., 2012. Megathrust asperities and clusters of slab dehydration identified by spatiotemporal characterization of seismicity below the Andean margin. *Geophys. J. Int.* 191, 923–931.
- Lin, A., Sun, Z., Yang, Z., 2003. Multiple generations of pseudotachylyte in the brittle to ductile regimes, Qinling-Dabie Shan ultrahigh-pressure metamorphic complex, central China. *Isl. Arc* 12, 423–435.
- Lund, M.G., Austrheim, H., 2003. High-pressure metamorphism and deep-crustal seismicity: evidence from contemporaneous formation of pseudotachylytes and eclogite facies coronas. *Tectonophysics* 372, 59–83.
- Maggi, M., Rossetti, F., Corfu, F., Theye, T., Andersen, T.B., Faccenna, C., 2012. Clinopyroxene-rutile phyllonites from the east tendra shear zone (Alpine Corsica, France): pressure-temperature-time constraints to the Alpine reworking of Variscan Corsica. *J. Geol. Soc.* 169, 723–732.
- Magott, R., 2016. Propagation de la rupture sismique dans la lithosphère océanique: une étude basée sur l'analyse structurale des cataclastes et pseudotachylytes jalonnant les failles dans les roches mafiques et ultramafiques accrétées ou obductées sur les continents. L'exemple corse. PhD thesis. Université de Bourgogne, Franche-Comté, p. 256.
- Magott, R., Fabbri, O., Fournier, M., 2016. Subduction zone intermediate-depth seismicity: insights from the structural analysis of Alpine high-pressure ophiolite-hosted pseudotachylytes (Corsica, France). *J. Struct. Geol.* 87, 95–114.
- Malavieille, J., Chemenda, A., Larroque, C., 1998. Evolutionary model for Alpine Corsica: mechanism for ophiolite emplacement and exhumation of high-pressure rocks. *Terra Nova* 10, 317–322.
- Manatschal, G., Froitzheim, N., Rubenach, M., Turrin, B.D., 2001. The role of detachment faulting in the formation of an ocean-continent transition: insights from the Iberia Abyssal Plain. *Geol. Soc.* 187, 405–428. London, Special Publications.
- Martin, L.A.J., Rubatto, D., Vitale-Brovarone, A., Hermann, J., 2011. Late Eocene

- lawsonite-eclogite facies metasomatism of a granitic sliver associated to ophiolites in Alpine Corsica. *Lithos* 125, 620–640.
- Mattauer, M., Proust, F., 1976. La Corse alpine: un modèle de genèse du métamorphisme haute pression par subduction de croûte continentale sous du matériel océanique. *Comptes Rendus Acad. Sci.* 282, 1249–1252.
- Mattauer, M., Proust, F., Etchecopar, A., 1977. Linéation “a” et mécanisme de cisaillement simple liés au chevauchement de la nappe des Schistes Lustrés en Corse. *Bull. Soc. Géol. Fr.* 4, 841–847.
- Mattauer, M., Faure, M., Malavieille, J., 1981. Transverse lineation and large-scale structures related to Alpine obduction in Corsica. *J. Struct. Geol.* 3, 401–409.
- McNulty, B.A., 1995. Pseudotachylytes generated in the semi-brittle and brittle regimes, Bench Canyon shear zone, central Sierra Nevada. *J. Struct. Geol.* 17, 1507–1521.
- Meresse, F., Lagabrielle, Y., Malavieille, J., Ildefonse, B., 2012. A fossil ocean-continent transition of the Mesozoic Tethys preserved in the schistes Lustrés nappe of northern Corsica. *Tectonophysics* 579, 4–16.
- Miranda, E., John, B.E., 2010. Strain localization along the Atlantis bank oceanic detachment fault system, Southwest Indian Ridge. *Geochem. Geophys. Geosyst.* 11, Q04002. <http://dx.doi.org/10.1029/2009GC002646>.
- Molli, G., Malavieille, J., 2011. Orogenic process and the Corsica/Apennine geodynamic evolution: insight from Taiwan. *Int. J. Earth Sci.* 100, 1207–1224. <http://dx.doi.org/10.1007/s00531-010-0598-y>.
- Moore, D.E., Lockner, D.A., Ma, S., Summers, R., Byerlee, J.D., 1997. Strengths of serpentinite gouges at elevated temperatures. *J. Geophys. Res. (Solid Earth)* 102, 14787–14801.
- Nadeau, R.M., Foxall, W., McEvilly, T.V., 1995. Clustering and periodic recurrence of microearthquakes on the San Andreas fault at Parkfield, California. *Science* 267, 503–507.
- Niemeijer, A., Di Toro, G., Nielsen, S., Di Felice, F., 2011. Frictional melting of gabbro under extreme experimental conditions of normal stress, acceleration, and sliding velocity. *J. Geophys. Res. (Solid Earth)* 116, B07404. <http://dx.doi.org/10.1029/2010JB008181>.
- Okada, T., Matsuzawa, T., Hasegawa, A., 2003. Comparison of source areas of M4.8 ± 0.1 repeating earthquakes off Kamaishi, NE Japan: are asperities persistent features? *Earth Planet. Sci. Lett.* 213, 361–374.
- Passchier, C., 1982. Pseudotachylyte and the development of ultramylonite bands in the Saint-barthélémy Massif, French pyrenees. *J. Struct. Geol.* 4, 69–79.
- Proctor, B.P., Mitchell, T.M., Hirth, G., Goldsby, D., Zorzi, F., Platt, J.D., Di Toro, G., 2014. Dynamic weakening of serpentinite gouges and bare surfaces at seismic slip rates. *J. Geophys. Res. (Solid Earth)* 119, 8107–8131. <http://dx.doi.org/10.1002/2014JB011057>.
- Reinen, L.A., Weeks, J.D., Tullis, T.E., 1991. The frictional behavior of serpentinite: implications for aseismic creep on shallow crustal faults. *Geophys. Res. Lett.* 18, 1921–1924.
- Reinen, L.A., Weeks, J.D., Tullis, T.E., 1994. The frictional behavior of lizardite and antigorite serpentinites: experiments, constitutive models, and implications for natural faults. *Pure Appl. Geophys.* 143, 317–358.
- Rossetti, F., Glodny, J., Theye, T., Maggi, M., 2015. Pressure-temperature-deformation-time of the ductile Alpine shearing in Corsica: from orogenic construction to collapse. *Lithos* 218–219, 99–116.
- Satake, K., Tanioka, Y., 1999. Sources of tsunami and tsunamigenic earthquakes in subduction zones. *Pure Appl. Geophys.* 154, 467–483.
- Scholz, C.H., 2002. *The Mechanics of Earthquake and Faulting*, second ed. Cambridge University Press, Cambridge, p. 471.
- Schroeder, T., John, B.E., 2004. Strain localization on an oceanic detachment fault system, Atlantis Massif, 30°N, Mid-Atlantic Ridge. *Geochem. Geophys. Geosyst.* 5, Q11007. <http://dx.doi.org/10.1029/2004GC000728>.
- Semmane, F., Cotton, F., Campillo, M., 2005. The 2000 Tottori earthquake: a shallow earthquake with no surface rupture and slip properties controlled by depth. *J. Geophys. Res. (Solid Earth)* 110, B03306. <http://dx.doi.org/10.1029/2004JB003194>.
- Seno, T., 2003. Fractal asperities, invasion of barriers, and interplate earthquakes. *Earth Planet Space* 55, 649–665.
- Sibson, R.H., 1980. Transient discontinuities in ductile shear zones. *J. Struct. Geol.* 2, 165–171.
- Sone, H., Shimamoto, T., Moore, D.E., 2012. Frictional properties of saponite-rich gouge from a serpentinite-bearing fault zone along the Gokasho-Arashima Tectonic Line, central Japan. *J. Struct. Geol.* 38, 172–182.
- Turco, E., Macchiavelli, C., Mazzoli, S., Schettino, A., Pierantoni, P.P., 2012. Kinematic evolution of Alpine Corsica in the framework of Mediterranean mountain belts. *Tectonophysics* 579, 193–206.
- Vitale-Brovarone, A., Beyssac, O., Malavieille, J., Molli, G., Beltrando, M., Compagnoni, R., 2013. Stacking and metamorphism of continuous segments of subducted lithosphere in a high-pressure wedge: the example of Alpine Corsica (France). *Earth-Sci. Rev.* 116, 35–56. <http://dx.doi.org/10.1016/j.earscirev.2012.10.003>.
- Vitale-Brovarone, A., Herwartz, D., 2013. Timing of HP metamorphism in the schistes Lustrés of Alpine Corsica: new Lu-Hf garnet and lawsonite ages. *Lithos* 172–173, 175–191.
- Vitale-Brovarone, A., Picatto, M., Beyssac, O., Lagabrielle, Y., Castelli, D., 2014. The blueschist-eclogite transition in the Alpine chain: P-T paths and the role of slow spreading extensional structures in the evolution of HP-LT mountain belts. *Tectonophysics* 615–616, 96–121.
- Yamanaka, Y., Kikuchi, M., 2004. Asperity map along the subduction zone in northeastern Japan inferred from regional seismic data. *J. Geophys. Res. (Solid Earth)* 109, B07307. <http://dx.doi.org/10.1029/2003JB002683>.
- Zechmeister, M.S., Ferré, E.C., Cosca, M.A., Geissman, J.W., 2007. Slow and fast deformation in the Dora Maira Massif, Italian Alps: pseudotachylytes and inferences on exhumation history. *J. Struct. Geol.* 29, 1114–1130.